PERGAMON

International Journal of Solids and Structures 40 (2003) 2215–2248

INTERNATIONAL JOURNAL OF SOLIDS and STRUCTURES

www.elsevier.com/locate/ijsolstr

Micro-stress prediction in composite laminates with high stress gradients

P. Hutapea [a], F.G. Yuan [a,*], N.J. Pagano [b]

[a] *Department of Mechanical and Aerospace Engineering, North Carolina State University, Raleigh, NC 27695, USA*
[b] *AFRL/MLBM Wright-Patterson AFB, OH 45433, USA*

Received 16 January 2002; received in revised form 3 December 2002

Abstract

The objective of this research is to develop a macroscopic theory, which can provide the connection between macro-mechanics and micro-mechanics in characterizing the micro-stress of composite laminates in regions of high macroscopic stress gradients. The micro-polar theory, a class of higher-order elasticity theory, of composite laminate mechanics is implemented in a well-known Pipes–Pagano free edge boundary problem. The micro-polar homogenization method to determine the micro-polar anisotropic effective elastic moduli is presented. A displacement-based finite element method based on micro-polar theory in anisotropic solids is developed in analyzing composite laminates. The effects of fiber volume fraction and cell size on the normal stress along the artificial interface resulting from ply homogenization of the composite laminate are also investigated. The stress response based on micro-polar theory is compared with those deduced from the micro-mechanics and classical elasticity theory. Special attention of the investigation focuses on the stress fields near the free edge where the high macro-stress gradient occurs. The normal stresses along the artificial interface and especially, the micro-stress along the fiber/matrix interface on the critical cell near the free edge where the high macro-stress gradient detected are the focus of this investigation. These micro-stresses are expected to dominate the failure initiation process in composite laminate. A micro-stress recovery scheme based on micro-polar analysis for the prediction of interface micro-stresses in the critical cell near the free edge is found to be in very good agreement with "exact" micro-stress solutions. It is demonstrated that the micro-polar theory is able to capture the micro-stress accurately from the homogenized solutions.

Keywords: Laminates; Stress; Micro-polar

1. Introduction

Development and application of fiber reinforced composites have already witnessed phenomenal growth over the past two decades. The prospect of controlling a wide range of material micro-structures and resulting properties has also been greatly enhanced. As the use of composite materials grows to include

* Corresponding author.
E-mail address: yuan@eos.ncsu.edu (F.G. Yuan).

0020-7683/02/$ - see front matter © 2002 Elsevier Science Ltd. All rights reserved.
doi:10.1016/S0020-7683(03)00018-0

structural components, which are essential to the function and safety of engineering structures, a major need in the design of these composite laminates is to assess acceptable stress levels under the conditions to be experienced during service. Efficient use of the remarkable properties of fiber composites will expand even more rapidly if the material micro-structure can further be precisely tailored to provide desired performance of composite structures.

The analysis of failure in fiber composites has traditionally followed two different levels of abstraction. The areas of investigation are known as *micro-mechanics* and *macro-mechanics*. The micro-mechanics approach aims at the involvement of microscopic inhomogeneities in various kinds of micro-failure processes by taking the composite micro-structure into account. The advantage of the micro-mechanics representation is that detailed information is directly obtained about the local interaction between the constituents and micro-failure mechanisms. The numerical modeling of exceedingly complicated geometric detail of all fibers and matrix, however, often requires exceedingly fine grids and hence results in excessive computer cost and capacity. The shear-lag model (Hedgepath, 1961; Hedgepath and Van Dyke, 1967; Chou, 1992) attempts to address this issue at a manageable level. However, this is done by oversimplifying the mechanical behavior of the constituents, which again leads to uncertain results. Even though many refinements have been incorporated into the shear-lag models (e.g. Hikami and Chou, 1990), further progress requires an alternative approach. It is immediately obvious that conducting a stress analysis in realistic composite laminates with the presence of million of fibers using this approach is an almost impossible task beyond the computational capacity of even the latest supercomputers. Hence, the micromechanical model is mainly restricted to the strength prediction at the lamina level or unidirectional composites. The micro-mechanics analyses suffer from two main limitations. First, they are not able to provide quantitative predictions of failure in composites. Second, they cannot be applied to problems of engineering design importance such as failure in the presence of free edges or holes, mainly because the interlaminar stresses have been neglected in the failure processes.

From the existing analytical approaches, it is clear that micro-mechanics approach alone will not explain the failure process of the laminates simply because the mutual interaction between the micro-stresses and "interlaminar" macro-stresses in the failure process has been totally neglected. While in the macromechanics approach, although the macroscopic or overall constitutive descriptions are developed from composite micro-structure in terms of the volume fraction, the shape, and the interface conditions of the constituents, the constitutive relations are independent of the scale of the micro-structure. Further, the effective-modulus theory, in principle, only applies to macroscopically uniform fields. Therefore, the stress fields near the high stress gradient regions using the classical approximation are unreliable (Pagano and Rybicki, 1974; Rybicki and Pagano, 1975; Pagano, 1978; Fish et al., 1993). Since the details of the generally complex, strongly heterogeneous micro-structures are not considered directly, the conventional macroscopic theory would inevitably involve erroneous theoretical predictions, and from which precise information of failure in the micro-level would be difficult to elicit.

None of the currently available macroscopic theories can provide the connection between micromechanics and macro-mechanics in characterizing the elastic response of composite laminates near edges and holes. The ultimate failure of laminates, which intertwines with the micro-failure mechanisms, has to be quantified to provide the necessary theoretical basis for design and application of composites to structures. Furthermore, a systematic failure analysis requires a methodology at the macro-level to correctly determine the stress distributions near the high stress gradient locations at the micro-level. In addition, there is clearly a need for more comprehensive experimental studies of micro-structural failure criteria, with emphasis on the requirements for applying predictive models to determine the ultimate load of the composite laminates.

Apparently, in regions of macroscopically steep stress (or strain) gradients such as free edges or holes, the conventional anisotropic elasticity theory utilizing the effective-modulus concept in the constitutive relations does not preserve the essential variation of the micro-stress distribution through the unit-cell at the micro-level. Indeed, rapid change of three-dimensional stress states contradicts the underlying as-

sumption of the macroscopically uniform state of stress from which the effective-modulus theory has been derived. As a consequence, at regions of high stress gradient the conventional approach ceases to provide true representation of physical reality. In order to represent the effect of the micro-stress variation through the unit cell and properly capture the meaningful macroscopic steep stress gradient fields, one must retain the volume average of the micro-stress distribution as the 'stress' acting on the cell but also the higher-order effects of the micro-stress distribution on the element. One of the higher-order effects of the micro-stress distribution is the set of first moments of micro-tractions, which provides couples on the surface of the cell. In a recent study of modeling the effective moduli of debonded interface by Yuan et al. (1997), it was found from micro-mechanics that the stresses on the boundary of the cell lead to resultant forces and moments, as in micro-polar (couple stress) theory. The couple stresses are conjugate to gradients of local rotation. Thus, in the elastic couple stress theory, the couple stresses are proportional to local rotation gradients, which are themselves proportional to differences of gradients of strain. This also results in the introduction of material lengths into the constitutive relations for dimensional consistency. Hence, the effect of absolute size of the micro-structure will be incorporated in the constitutive description. The presence of the length parameter, in turn, implies that the micro-polar theory encompasses the size effects that are ignored in the classical anisotropic elasticity theory.

The couple stress concept shown in Fig. 1 is due to Voigt (1887) and was further developed by the Cosserat and Cosserat (1909). Following the work by Mindlin and Tiersten (1962) on linear micro-polar elasticity, a number of stress concentration problems have been investigated (e.g. Mindlin, 1963). The effect of couple stresses on the singular stress concentrations in elastic solids has been explored (Muki and Sternberg, 1965; Sternberg and Muki, 1967; Sternberg, 1968; Pagano and Sih, 1968; Bogy and Sternberg, 1968; Savin and Nemish, 1968; Atkinson and Leppington, 1977). Several pathological predictions of classical elasticity in singular stress concentration problems are altered, mitigated, or possibly eliminated when couple stresses are taken into account. A Cosserat continuum and the theory of elasticity with micro-structure have

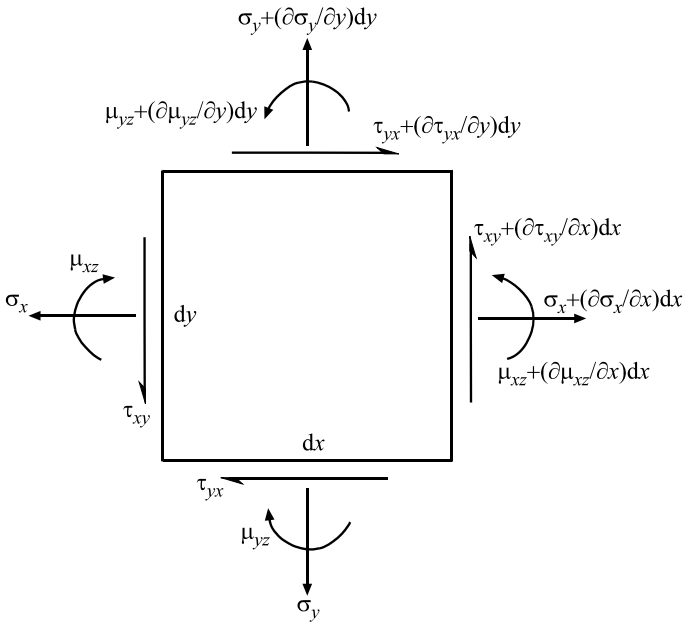

Fig. 1. 2D Cartesian componets of stress and couple stress.

been suggested as analytical models describing the dynamic behavior of composite materials (e.g. monograph by Achenbach, 1973).

The research on finite element formulation of micro-polar theory is also limited due to the lack of study in defining micro-polar shear moduli. Many researchers avoid the nonexistent of shear moduli by simplifying or remodeling the micro-polar problem. For example, Wood (1988) used a complementary-based variational principle to solve plane linear elastic couple-stress problems. The principle is analogous to that used in a total potential energy-based Mindlin/Reissner thick plate bending analysis and as such is a generalization of the classical analogy between plate stretching and plate bending. Parametric studies of micro-polar theory also have been conducted. For example, Nakamura et al. (1984, 1988) developed the total potential energy for a body composed of an anisotropic micro-polar linear elastic material and formulated a displacement-type finite element model. The program is verified by computing the stress concentration around a hole in an isotropic micro-polar material for which an exact analytical solution exists. Several anisotropic material cases are presented which demonstrate the dependence of the stress concentration factor on the micro-polar material parameters. Very recently, Forest and Sab (1998) proposed an alternative methodology consisting in replacing the heterogeneous medium by a generalized continuum. Such continua involve additional degrees of freedom (Cosserat media) or higher-order gradients of the displacement field (second grade materials). In general, they replaced a composite material with a homogenous generalized continuum by developing the macroscopic displacement field into a polynomial main field and a periodic perturbation. Forest (1998) provided a method to derive micro-polar shear moduli of composites. He modeled a cluster of nine cells and applied rotation at the center cell to simulate the deformation of micro-polar media.

It is clear that a higher-order continuum theory such as micro-polar theory may provide a significant improvement in analyzing the stress behavior of composite structures near the steep stress gradient zone, and further predicting the micro-stress near this region where the failure may initiate in this micro-scale. Therefore, there is a need to implement micro-polar theory into the ply level in the laminate analysis. Firstly, emphasis is placed on deriving micro-polar composite moduli and assessing the singular behavior of stresses in the regions close to the exposed free edge. A finite element technique to derive these moduli is presented. The effects of micro-polar theory on the normal stresses along the ''artificial'' interface that is an artifact of ply homogenization, particularly near the high macro-stress gradient region, are also examined. Secondly, the micro-stress along the fiber–matrix interface of the 'critical' cell are of interest. 'Critical' cell is defined as the cell on the interface of matrix and composite and near the free edge of the lamina, where the high macro-stress gradient is found due to material and/or geometric discontinuity.

2. Formulation

A class of free edge problems which involve stress intensification near the edge in the composite laminate has been presented by Pipes and Pagano (1970), Pagano (1974a,b), Wang and Yuan (1983). In general, the displacement field is given by

$$\begin{aligned} u(x,y,z) &= U(x,y) \\ v(x,y,z) &= V(x,y) \\ w(x,y,z) &= W(x,y) + \varepsilon_z z \\ \phi(x,y,z) &= \phi(x,y) \end{aligned} \tag{2.1}$$

where u, v and w are the x, y, z components of displacements, respectively, ϕ is the independent rotation, and ε_z is an applied uniform strain in the z-direction. Thus all the stresses are function of x and y alone. The resulting generalized plane deformation problems in elasticity is solved by means of finite element code

ANSYS. For the boundary value problem modeled by micro-polar elasticity, the problem is solved by use of finite element code as discussed in Appendix A. In ANSYS, the axial strain ε_z is imposed on the finite element problem by simulating it as thermal strain in z plane strain formulation:

$$\varepsilon_z = \alpha_z T \tag{2.2}$$

where α_z is the thermal expansion coefficient and T is the temperature rise.

Two cases of free edge boundary value problems are considered in this study. Due to the symmetry in geometry and the lay-up, only a quarter is the laminate is modeled. The first case is a six-layered laminate with fibrous lamina with fiber volume fraction, 30.7%. One quarter of the cross-section of a composite consists of two fibrous layers with eight fibers and an epoxy layer is shown in Fig. 2. The size of each cell is 160 μm and the fiber diameter is 100 μm. The intention of using this configuration with eight fibers allows the model to take every heterogeneity in a lamina into account for the numerical modeling. For each boundary value problem, the solutions from micro-mechanics model (MM), effective modulus (homogenization) model (EM) and micro-polar model (MP) will be determined and then studied. The micro-stress solutions from this micro-mechanics model will serve as reference "exact" solutions that will be compared with those obtained by the EM and MP solutions. In the MM model, the fibers and matrix are recognized explicitly in the numerical modeling; EM and MP solutions are modeled by replacing the fibrous and matrix layers by their respective effective moduli. The derivation of effective moduli for classical elasticity and micro-polar elasticity is presented in Section 3. The constituent moduli are in the following: $\varepsilon_z = 0.002$, Sigma 1240 (silicon carbide) fibers have $E = 325$ GPa, $v = 0.15$, and epoxy matrix has $E = 3.45$ GPa, $v = 0.35$.

As shown in Fig. 2, the cell size is h. The elasticity boundary conditions on the center line and free edge are given by

$$u(0, y) = \sigma_{xy}(0, y) = \sigma_{xy}(4h, y) = \sigma_x(4h, y) = 0 \tag{2.3}$$

while on the central plane and upper surface, we have

$$v(x, 0) = \sigma_{xy}(x, 0) = \sigma_{xy}(x, 3h) = \sigma_y(x, 3h) = 0 \tag{2.4}$$

In the MP model, additional boundary conditions are prescribed.

$$\phi_z(x, 0) = \phi_z(0, y) = \mu_{xz}(4h, y) = 0 \tag{2.5}$$

Note that the epoxy layer is modeled by the classical effective moduli. In this layer, $\phi_z = 0$. In all the cases, particular emphasis will be placed on the cell centered at $(3.5h, 1.5h)$ (called 'critical' cell), i.e., the cell in which the EM and MP singularities exist.

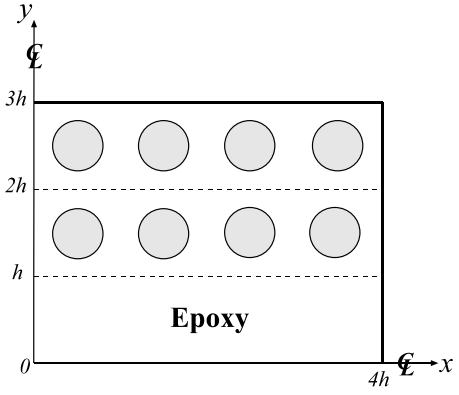

Fig. 2. Two-row composite lamina with fiber diameter: 100 μm and cell size: 160 μm × 160 μm.

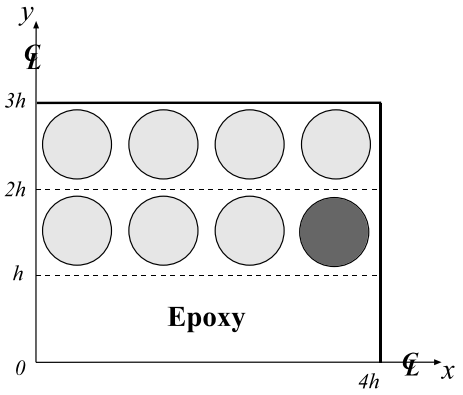

Fig. 3. Two-row composite lamina with fiber diameter: 141.42 μm and cell size: 160 μm × 160 μm.

The second boundary value problem is similar to that of the first problem except that a higher fiber volume fraction 61.4% is used. The quarter region is shown in Fig. 3. The boundary conditions are the same as in Eqs. (2.3) and (2.4). The same constituent moduli are also used in the second problem.

An ANSYS and finite element code are developed to analyze the stresses and displacements for MM, EM and MP models. Eight-node isoparametric elements are used in these modeling. For modeling MM, EM and MP models under axial strain ε_z, the loading is simulated as a thermoelastic problem with thermal expansion coefficients, $\alpha_1 = \alpha_2 = 0$ and $\alpha_3 = \varepsilon_z$ under unit temperature rise. The finite element procedure of the micro-polar theory for this boundary value problem is described in Appendix A.

3. Prediction of micro-polar composite moduli

A finite element approach to calculate micro-polar moduli in orthotropic solids is presented. A square fibrous unit cell is employed in the analysis. Since the unit cell possesses a center of symmetry, there will be no coupling between the overall micro-polar deformation and curvatures. The derivation of the moduli in this study contains three parts. Firstly, effective elastic moduli deduced from the classical homogenized scheme are obtained based on the representative volume element (RVE) concept as presented by Yuan et al. (1997). Secondly, a cluster of cells suggested by Forest (1998) is used together with traction continuity and displacement continuity conditions along the boundary of the center cell for determining the micro-polar shear moduli. Finally, determination of bending moduli of the unit cell from a long strip of periodic cells using a least squares method or finite element method is proposed. The finite element method by means of ANSYS software package is utilized.

For an orthotropic micro-polar solid under generalized plane deformation, constitutive equations for this class of problems are expressed as

$$\begin{Bmatrix} \bar{\sigma}_{xx} \\ \bar{\sigma}_{yy} \\ \bar{\sigma}_{zz} \\ \bar{\sigma}_{xy} \\ \bar{\sigma}_{yx} \\ \bar{\mu}_{xz} \\ \bar{\mu}_{yz} \end{Bmatrix} = \begin{bmatrix} C_{11} & C_{12} & C_{13} & 0 & 0 & 0 & 0 \\ C_{12} & C_{22} & C_{23} & 0 & 0 & 0 & 0 \\ C_{13} & C_{23} & C_{33} & 0 & 0 & 0 & 0 \\ 0 & 0 & 0 & G_{11} & G_{12} & 0 & 0 \\ 0 & 0 & 0 & G_{12} & G_{22} & 0 & 0 \\ 0 & 0 & 0 & 0 & 0 & B_{11} & B_{12} \\ 0 & 0 & 0 & 0 & 0 & B_{12} & B_{22} \end{bmatrix} \begin{Bmatrix} \bar{\varepsilon}_{xx} \\ \bar{\varepsilon}_{yy} \\ \bar{\varepsilon}_{zz} \\ \bar{\varepsilon}_{xy} \\ \bar{\varepsilon}_{yx} \\ \bar{\kappa}_{xz} \\ \bar{\kappa}_{yz} \end{Bmatrix} \tag{3.1}$$

The strain–displacement relations are

$$\bar{\varepsilon}_{xx} = \frac{\partial \bar{u}}{\partial x}, \quad \bar{\varepsilon}_{yy} = \frac{\partial \bar{v}}{\partial y}, \quad \bar{\varepsilon}_{zz} = \frac{\partial \bar{w}}{\partial z}, \quad \bar{\varepsilon}_{xy} = \frac{\partial \bar{v}}{\partial x} - \bar{\phi}_z, \quad \bar{\varepsilon}_{yx} = \frac{\partial \bar{u}}{\partial x} + \bar{\phi}_z$$

where the bar on the stresses and strains denote the averaged quantities, ϕ_z is the micro-polar rotation, μ_{xz} and μ_{yz} are couple stresses, and κ_{xz} and κ_{yz} are the curvatures.

The classical orthotropic constants, C_{ij} $(i,j=1,2,3)$, are deduced from three extension and one shear boundary value problem with periodic boundary conditions to obtain shear moduli. In addition to the shear test, a cluster of nine composite cells is employed to simulate the micro-polar shear force that is activated by a rotation of a center cell. By applying this method, the anti-symmetric shear stress condition will be automatically satisfied. Using shear and rotation tests, the micro-polar shear moduli, G_{ij} $(i,j=1,2)$, are determined. Since there is no RVE in the micro-polar theory, bending moduli, B_{ij} $(i,j=1,2)$, are approximated by applying bending deformation to a long strip of unit cells. The Young's modulus, Poisson's ratios, in-plane and longitudinal shear moduli of the composite are determined by the elastic properties of the constituents and internal geometry of the RVE (Yuan et al., 1997). Only the derivation of micro-polar shear and bending moduli are presented in this paper.

3.1. Shear test—in-plane composite shear modulus

For the composite under shear, straight cell boundaries may not remain straight after the composite has been deformed. Since the boundary displacements and traction on any cells must be compatible with those on the neighboring cells, for the finite element modeling, constraints are imposed on the displacements at the edges $x =$ constant and $y =$ constant of the cell boundary where the displacements are not necessarily linear. Applying the boundary conditions into a quarter cell model as derived in Yuan et al. (1997):

$$\begin{aligned} &x = 0, \quad v(0,y) = \sigma_x(0,y) = 0 \\ &x = a, \quad v(a,y) = \frac{1}{2} a \gamma^{\circ}_{xy}, \quad \sigma_x(0,y) = 0 \\ &y = 0, \quad u(x,0) = \sigma_y(x,0) = 0 \\ &y = b, \quad u(x,b) = \frac{1}{2} b \gamma^{\circ}_{xy}, \quad \sigma_y(x,b) = 0 \end{aligned} \tag{3.2}$$

From the constitutive equation, we can express the effective shear constitutive equation in the following way

$$\begin{Bmatrix} \bar{\sigma}_{xy} \\ \bar{\sigma}_{yx} \end{Bmatrix} = \begin{bmatrix} G_{11} & G_{12} \\ G_{12} & G_{22} \end{bmatrix} \begin{Bmatrix} \bar{\varepsilon}_{xy} \\ \bar{\varepsilon}_{yx} \end{Bmatrix} \tag{3.3}$$

$$\begin{Bmatrix} \bar{\varepsilon}_{xy} \\ \bar{\varepsilon}_{yx} \end{Bmatrix} = \frac{1}{G_{11}G_{22} - G_{12}^2} \begin{bmatrix} G_{22} & -G_{12} \\ -G_{12} & G_{11} \end{bmatrix} \begin{Bmatrix} \bar{\sigma}_{xy} \\ \bar{\sigma}_{yx} \end{Bmatrix} \tag{3.4}$$

Adding the two shear strains in Eq. (3.4) yields

$$\bar{\varepsilon}_{xy} + \bar{\varepsilon}_{yx} = \frac{\partial \bar{v}}{\partial x} + \frac{\partial \bar{u}}{\partial y} = \frac{(G_{22} - G_{12})\bar{\sigma}_{xy} + (-G_{12} + G_{11})\bar{\sigma}_{yx}}{G_{11}G_{22} - G_{12}^2} \tag{3.5}$$

For classical elasticity problem, the shear stress is symmetric, $\bar{\sigma}_{xy} = \bar{\sigma}_{yx}$. Therefore, Eq. (3.5) can be simplified as follows.

$$\bar{\sigma}_{xy} = \frac{G_{12}^2 - G_{11}G_{22}}{2G_{12} - G_{11} - G_{22}}\bar{\gamma}_{xy} \tag{3.6}$$

The composite in-plane shear modulus is defined as:

$$\bar{\sigma}_{xy} = G_{12}^{*}\bar{\gamma}_{xy} \tag{3.7}$$

The average of the in-plane shear stress in the RVE:

$$\bar{\sigma}_{xy} = \frac{1}{b}\int_0^b \sigma_{xy}(a,y)\,\mathrm{d}y \tag{3.8}$$

The average of the in-plane shear strain is derived in Yuan et al. (1997):

$$\bar{\gamma}_{xy} = \gamma_{xy}^{\circ} \tag{3.9}$$

Denote the shear modulus of elasticity, G_{12}^{*}, as follows.

$$G_{12}^{*} = \frac{G_{12}^2 - G_{11}G_{22}}{2G_{12} - G_{11} - G_{22}} \tag{3.10}$$

Applying Eqs. (3.3) and (3.6), G_{12}^{*} can be determined. It also can be proven that $\bar{\sigma}_x = \bar{\sigma}_y = \bar{\sigma}_z = 0$. Therefore, shear coupling coefficients are identically zero, i.e.,

$$C_{16} = C_{26} = C_{36} = 0 \tag{3.11}$$

3.2. Center-rotation test—rotation modulus

In micro-polar theory, the translational and rotational degrees of freedom are independent of each other. The translation describes the displacement of the center of the unit cell whereas the global rotation of each unit cell is accounted for by the additional degrees of freedom. The neighboring cells will oppose resistance to inner rotation. We consider the anti-symmetric part of strain in micro-polar theory is introduced by a mechanism of cell rotation, which is not considered in the conventional theory of elasticity. Non-symmetrical shear stress for the cell results from the rotation of the center cell, which activates shear forces transmitted through cell contacts. Thus, for the determination of moduli G_{11}, G_{22} and G_{12}, rotation can be considered in addition to the shear test. The center of the cells is fixed and a rigid rotation is prescribed at the boundary of the center cell. This rotation corresponds to a non-vanishing relative rotation of the micro-structure (anti-symmetric strains). The finite element computation provides the reaction forces on each sides of the center cell that represent the resistance of the material to inner rotation.

The displacement boundary conditions for the center cell are given by:

$$\begin{aligned} u(a,y) &= u(-a,y) \\ v(a,y) &= v(-a,y) + a\gamma^{\circ} \\ u(x,b) &= u(x,-b) - b\gamma^{\circ} \\ v(x,b) &= v(x,-b) \end{aligned} \tag{3.12}$$

For the remaining eight cells, the displacement is fixed at their centers (i.e., $u = v = 0$). Due to the symmetric geometry of the cell under constraint Eq. (3.12), we have

$$\begin{aligned} \varepsilon_x(x,y) &= -\varepsilon_x(x,-y) \\ \varepsilon_y(x,y) &= -\varepsilon_y(x,-y) \\ \gamma_{xy}(x,y) &= \gamma_{xy}(x,-y) \end{aligned} \tag{3.13}$$

Integrating the strain–displacement relation in conjunction with Eq. (3.13) and then applying Eq. (3.12) give

$$u(x,0) = v(0,y) = 0 \tag{3.14}$$

Thus, there is no translation at the center of the center cell.

Following Yuan et al. (1997), we can prove that

$$\begin{aligned} &\bar{\sigma}_x = \bar{\sigma}_y = \bar{\sigma}_z = 0 \\ &\bar{\varepsilon}_x = \bar{\varepsilon}_y = \bar{\varepsilon}_z = 0 \end{aligned} \tag{3.15}$$

It can be readily shown that

$$\bar{\varepsilon}_{(xy)} = \bar{\gamma}_{xy} = \frac{\bar{\varepsilon}_{xy} + \bar{\varepsilon}_{yx}}{2} = \frac{1}{2a}\int_{-a}^{a} \frac{\partial v(x,b)}{\partial x}\,\mathrm{d}x + \frac{1}{2b}\int_{-b}^{b} \frac{\partial u(a,y)}{\partial y}\,\mathrm{d}y = 0 \tag{3.16}$$

The average local rotation for the center cell relative to the surrounding cells is

$$\bar{\phi}_z = \frac{1}{4ab}\int_A \frac{1}{2}\left(\frac{\partial v}{\partial x} - \frac{\partial u}{\partial y}\right)\mathrm{d}x\,\mathrm{d}y = \frac{\gamma^{\circ}}{2} \tag{3.17}$$

Rigid body rotation, ω_z, can be estimated from rotation of the rigid Cartesian axes located at the center of the center cell.

$$\omega_z = \frac{1}{2}\left(\frac{\partial v}{\partial x} - \frac{\partial u}{\partial y}\right)\Bigg|_{\substack{x=0 \\ y=0}} \tag{3.18}$$

By taking advantage of Eq. (3.14), ϕ_z can be readily calculated from either one of the axis. The anti-symmetric shear strain can be obtained:

$$\bar{\varepsilon}_{[xy]} = \frac{1}{2}(\bar{\varepsilon}_{xy} - \bar{\varepsilon}_{yx}) = \omega_z - \bar{\phi}_z \tag{3.19}$$

For a square fibrous cell with the symmetry about x and y the axes, $G_{11} = G_{22}$. From Eq. (3.3) with the help of Eq. (3.16), we obtain

$$\bar{\sigma}_{xy} + \bar{\sigma}_{yx} = 2\bar{\sigma}_{(xy)} = 0 \tag{3.20}$$

Eq. (3.3) further leads to

$$\bar{\sigma}_{[xy]} = \frac{1}{2}(\bar{\sigma}_{xy} - \bar{\sigma}_{yx}) = (G_{11} - G_{12})\left[\frac{1}{2}(\bar{\varepsilon}_{xy} - \bar{\varepsilon}_{yx})\right] = (G_{11} - G_{12})\bar{\varepsilon}_{[xy]} \tag{3.21}$$

and Eq. (3.6) gives:

$$G_{12}^{*} = G_{11} + G_{12} \tag{3.22}$$

The physical meaning of elasticity and micro-rotations with regards to the anti-symmetric shear stress is explained more clearly in Fig. 4. To simulate the micro-polar deformation, Eq. (3.12) is applied to the center cell. For the cluster of cells with fixed centers, the prescribed rigid body rotation activates shear forces that cause the anti-symmetric part of shear stresses for the center cell. The reactive shear forces are extracted from each side of the cell to calculate the shear stress.

The value of $\bar{\sigma}_{[xy]}$ can be obtained from the boundaries of the center cell shown in Fig. 4. Then, utilizing Eqs. (3.19), (3.21) and (3.22), the micro-polar shear moduli can be obtained.The resulting deformation is shown in Fig. 5.

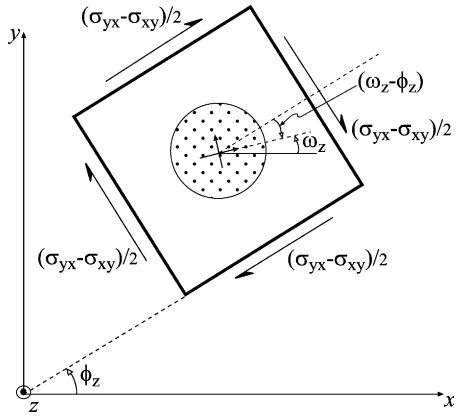

Fig. 4. Kinematics of macro- and micro-rotations in micro-polar solids.

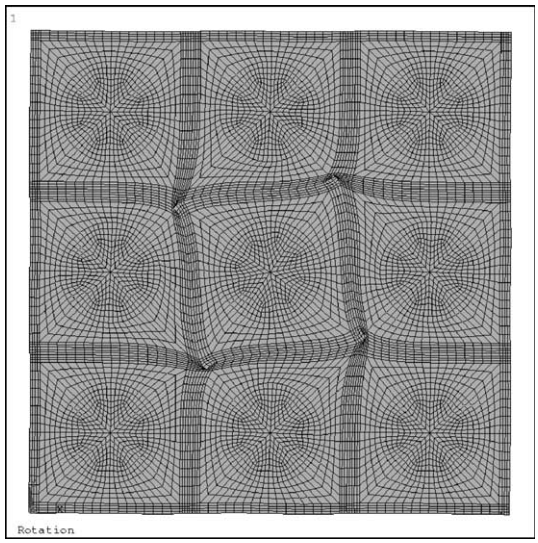

Fig. 5. Nine-cell model of fibrous cells for calculating rotational modulus using micro-polar theory.

Under the displacement boundary conditions, Eq. (3.12), the strain energy density can be expressed by

$$U = \frac{1}{2}\bar{\sigma}_{xy}\bar{\varepsilon}_{xy} + \frac{1}{2}\bar{\sigma}_{yx}\bar{\varepsilon}_{yx} = \bar{\sigma}_{(xy)}\bar{\varepsilon}_{(xy)} + \bar{\sigma}_{[xy]}\bar{\varepsilon}_{[xy]} = \bar{\sigma}_{(xy)}\bar{\varepsilon}_{(xy)} + \bar{\sigma}_{[xy]}(\omega_z - \bar{\phi}_z) \tag{3.23}$$

The first term in Eq. (3.23) is the energy produced by the symmetric shear stress undergoing shear distortion; the second term represents the energy by the anti-symmetric shear stress $\bar{\sigma}_{[xy]}$ undergoing a deformation due to the relative rotation $(\omega_z - \bar{\phi}_z)$.

Using (3.16) and (3.20), Eq. (3.23) can be rewritten as

$$U = \frac{1}{2}(\sigma_{xy} - \sigma_{yx})(\omega_z - \bar{\phi}_z) \tag{3.24}$$

3.3. Bending deformation—modulus of curvature

Consider a long strip of unit cells in the x-direction. The displacement compatibility equations for the cells under bending deformation on the surfaces $x = \pm a$ are:

$$\begin{aligned} u(a,y) &= u(-a,y) - 2a\kappa^{\circ}_{xz}y \\ v(a,y) &= v(-a,y) \\ u(x,b) &= u(x,-b) - 2b\kappa^{\circ}_{xz}x \\ v(x,b) &= v(x,-b) \end{aligned} \tag{3.25}$$

The traction continuity conditions among neighboring horizontal cells regardless of the loading and the traction-free condition along $y = \pm b$ are given as

$$\begin{aligned} \sigma_x(a,y) &= \sigma_x(-a,y) \\ \sigma_{xy}(a,y) &= \sigma_{xy}(-a,y) \\ \sigma_y(x,b) &= \sigma_y(x,-b) = 0 \\ \sigma_{xy}(x,b) &= \sigma_{xy}(x,-b) = 0 \end{aligned} \tag{3.26}$$

First considering the anti-symmetry about the x-axis

$$\begin{aligned} \varepsilon_x(x,y) &= -\varepsilon_x(x,-y) \\ \varepsilon_y(x,y) &= -\varepsilon_y(x,-y) \\ \gamma_{xy}(x,y) &= \gamma_{xy}(x,-y) \end{aligned} \tag{3.27}$$

Integrating Eq. (3.27) and imposing the fixed displacements and rotation at the center of the cell element, we obtain

$$\begin{aligned} u(x,y) &= -u(x,-y) \\ v(x,y) &= v(x,-y) \end{aligned} \tag{3.28}$$

Thus

$$u(x,0) = 0 \tag{3.29}$$

Using (3.28a), Eq. (3.25c) reduces to

$$u(x,b) = -b\kappa^{\circ}_{xz}x \tag{3.30}$$

From Eq. (3.27),

$$\begin{aligned} \sigma_x(x,y) &= -\sigma_x(x,-y) \\ \sigma_y(x,y) &= -\sigma_y(x,-y) \\ \sigma_{xy}(x,y) &= \sigma_{xy}(x,-y) \end{aligned} \tag{3.31}$$

Thus,

$$\sigma_x(x,0) = 0, \quad \sigma_y(x,0) = 0 \tag{3.32}$$

Consequently, the cells can be modeled by a half of the region

$$y = 0 \begin{cases} u(x,0) = 0 \\ \sigma_x(x,0) = 0 \\ \sigma_y(x,0) = 0 \end{cases}, \quad y = b \begin{cases} u(x,b) = -b\kappa^{\circ}_{xz}x \\ \sigma_{xy}(x,b) = 0 \\ \sigma_y(x,b) = 0 \end{cases} \tag{3.33}$$

Then considering the symmetry about the y-axis

$$\begin{aligned}\varepsilon_x(x,y) &= \varepsilon_x(-x,y)\\ \varepsilon_y(x,y) &= \varepsilon_y(-x,y)\\ \gamma_{xy}(x,y) &= -\gamma_{xy}(-x,y)\end{aligned} \tag{3.34}$$

Integrating Eq. (3.34) and imposing the fixed displacements and rotation at the center of the cells, we obtain

$$\begin{aligned}u(x,y) &= -u(-x,y)\\ v(x,y) &= v(-x,y)\end{aligned} \tag{3.35}$$

Thus,

$$u(0,y) = 0 \tag{3.36}$$

Using Eq. (3.35a), Eq. (3.25a) reduces to

$$u(a,y) = -u(-a,y) = -a\kappa^{\circ}_{xz} y \tag{3.37}$$

From Eq. (3.34),

$$\begin{aligned}\sigma_x(x,y) &= \sigma_x(-x,y)\\ \sigma_y(x,y) &= \sigma_y(-x,y)\\ \sigma_{xy}(x,y) &= -\sigma_{xy}(-x,y)\end{aligned} \tag{3.38}$$

Therefore,

$$\sigma_{xy}(0,y) = 0 \tag{3.39}$$

Using Eqs. (3.38c) and (3.26b),

$$\sigma_{xy}(a,y) = 0 \tag{3.40}$$

From Eqs. (3.40), (3.26b) and (3.37), we obtain

$$\frac{\partial v(a,y)}{\partial x} = -\frac{\partial v(a,y)}{\partial x} = a\kappa^{\circ}_{xz} \tag{3.41}$$

Thus, the overall problem can be modeled by a quarter of the region with Eq. (3.33) and the following conditions

$$x = 0 \begin{cases} u(0,y) = 0 \\ \sigma_{xy}(0,y) = 0 \end{cases}, \quad x = a \begin{cases} u(a,y) = -a\kappa^{\circ}_{xz} y \\ \sigma_{xy}(a,y) = 0 \end{cases} \tag{3.42}$$

Using Gauss theorem together with Eqs. (3.25), (3.28) and (3.35) leads to

$$\bar{\varepsilon}_x = 0, \quad \bar{\varepsilon}_y = 0, \quad \bar{\gamma}_{xy} = 0, \quad \bar{\kappa}_y = 0 \tag{3.43}$$

The above equation demonstrates the pure bending state under the constraints Eq. (3.42).

Further using Gauss theorem with Eqs. (3.25) and (3.41) yields

$$\bar{\kappa}_{xz} = \kappa^{\circ}_{xz} \tag{3.44}$$

The average couple stress is obtained as

$$\bar{\mu}_{xz} = \frac{1}{2b}\int_{-b}^{b} y\sigma_x \,\mathrm{d}y \tag{3.45}$$

The modulus of curvature is defined as

$$\bar{\mu}_{xz} = B_{11}\kappa^{\circ}_{xz} \tag{3.46}$$

Similarly, by applying the bending deformation along $y = \pm b$ with a vertical strip of cells, we have

$$\bar{\mu}_{yz} = B_{22}\kappa^{\circ}_{yz} \tag{3.47}$$

where $B_{22} = B_{11}$. This approach will always lead to $B_{12} = 0$.

The above boundary value problem can be solved by finite element method. In the following, another method using a least squares method by Hulbert and Rybicki (1971) is examined. The use of boundary collocation method will serve two purposes: (1) to compare the solutions with those obtained from finite element method, (2) to determine the bending moduli under the applied loading conditions.

An elastic approach is used to solve this problem. Referring to a polar coordinate system, the basic field equations for the plane strain problems are:

Strain–displacement relations:

$$\varepsilon_r = \frac{\partial u_r}{\partial r}, \quad \varepsilon_\theta = \frac{1}{r}\frac{\partial u_\theta}{\partial \theta} + \frac{u_r}{r}, \quad \gamma_{r\theta} = \frac{1}{r}\frac{\partial u_r}{\partial \theta} + \frac{\partial u_\theta}{\partial r} - \frac{u_\theta}{r} \tag{3.48}$$

Constitutive equations of isotropic materials:

$$\varepsilon_r = \frac{1}{E'}(\sigma_r - \nu'\sigma_\theta), \quad \varepsilon_\theta = \frac{1}{E'}(\sigma_\theta - \nu'\sigma_r), \quad \gamma_{r\theta} = \frac{1}{G'}\sigma_{r\theta} \tag{3.49}$$

where $E' = \frac{E}{1-\nu^2}$, $\nu' = \frac{\nu}{1-\nu}$.

Equilibrium equations:

$$\begin{aligned} &\frac{\partial \sigma_r}{\partial r} + \frac{1}{r}\frac{\partial \sigma_{r\theta}}{\partial \theta} + \frac{\sigma_r - \sigma_\theta}{r} = 0 \\ &\frac{\partial \sigma_{r\theta}}{\partial r} + \frac{1}{r}\frac{\partial \sigma_\theta}{\partial \theta} + \frac{2\sigma_{r\theta}}{r} = 0 \end{aligned} \tag{3.50}$$

Introducing the Airy stress function Φ, and expressing stresses as

$$\sigma_r = \frac{1}{r}\left(\frac{\partial \Phi}{\partial r} + \frac{1}{r}\frac{\partial^2 \Phi}{\partial \theta^2}\right), \quad \sigma_\theta = \frac{\partial^2 \Phi}{\partial r^2}, \quad \sigma_{r\theta} = -\frac{\partial}{\partial r}\left(\frac{1}{r}\frac{\partial \Phi}{\partial \theta}\right) \tag{3.51}$$

the equilibrium equations are automatically satisfied.

For the doubly connected matrix region with symmetry along the y-axis, the stress function in the matrix can be assumed as

$$\Phi^{(\mathrm{m})} = \left(b_1^{(\mathrm{m})} r^3 + a_{-1}^{(\mathrm{m})} r^{-1}\right)\sin\theta + \sum_{n=2}^{N}\left(a_n^{(\mathrm{m})} r^n + a_{-n}^{(\mathrm{m})} r^{-n} + b_n^{(\mathrm{m})} r^{n+2} + b_{-n}^{(\mathrm{m})} r^{-n+2}\right)\sin n\theta \tag{3.52}$$

For the simply connected fiber region symmetrical about the y-axis, the stress function is expressed by

$$\Phi^{(\mathrm{f})} = b_1^{(\mathrm{f})} r^3 \sin\theta + \sum_{n=2}^{N}\left(a_n^{(\mathrm{f})} r^n + b_n^{(\mathrm{f})} r^{n+2}\right)\sin n\theta \tag{3.53}$$

In the above Eqs. (3.52) and (3.53), the superscripts f and m in the bracket denote the fiber and matrix regions respectively. Note that in order to solve the bending deformation along the $x = \pm a$, the odd sine terms in Eq. (3.52) and (3.53) are chosen so that the anti-symmetric condition at $\theta = 0$ and the symmetric condition at $\theta = \pi/2$ are fulfilled.

With the series chosen which exactly satisfies symmetrical conditions along the y-axis and anti-symmetric conditions on x-axes, there remains in the problem the necessity of satisfying the following prescribed surface conditions and fiber–matrix interface conditions for the rectangular cell

$$u^{(\mathrm{m})}(a,y) = -a\kappa^{\circ}_{xz} y \tag{3.54}$$

$$u^{(\mathrm{m})}(x,b) = -b\kappa^{\circ}_{xz} x \tag{3.55}$$

$$\sigma_r^{(\mathrm{m})} - \sigma_r^{(\mathrm{f})} = 0, \quad \sigma_{r\theta}^{(\mathrm{m})} - \sigma_{r\theta}^{(\mathrm{f})} = 0, \quad \text{at } r = R \tag{3.56}$$

$$u_r^{(\mathrm{m})} - u_r^{(\mathrm{f})} = 0, \quad u_\theta^{(\mathrm{m})} - u_\theta^{(\mathrm{f})} = 0, \quad \text{at } r = R \tag{3.57}$$

$$\sigma_{xx}^{(\mathrm{m})}(a,y) = \sigma_{xy}^{(\mathrm{m})}(x,b) = 0 \tag{3.58}$$

where R is the fiber radius and

$$u = u_r \cos\theta - u_\theta \sin\theta$$

$$\sigma_{xx} = \sigma_{rr}\cos^2\theta + \sigma_{\theta\theta}\sin^2\theta - 2\sigma_{r\theta}\sin\theta\cos\theta$$

$$\sigma_{yy} = \sigma_{rr}\sin^2\theta + \sigma_{\theta\theta}\cos^2\theta + 2\sigma_{r\theta}\sin\theta\cos\theta$$

$$\sigma_{xy} = (\sigma_{rr} - \sigma_{\theta\theta})\sin\theta\cos\theta + \sigma_{r\theta}(\cos^2\theta - \sin^2\theta)$$

A least squares method is utilized to evaluate the coefficients of the truncated series terms so that the stress and displacement fields can be obtained. The method is carried out in the following steps:

(1) select a set of discrete points on the cell surface ($x = a$ and $y = b$) and the fiber–matrix interface;
(2) apply the prescribed boundary conditions on the cell surface and interface continuity conditions, Eqs. (3.54)–(3.58), to these discrete points;
(3) solve the resulting set of simultaneous equations for the coefficients.

The total number of discrete points is chosen so that the number of equations, m, is greater than the number of unknowns, n. The solutions can be obtained by solving the overdetermined set of equations in the least squares sense.

For the above displacement boundary conditions, after solving the equations the couple stress is determined by

$$\bar{\mu}_{xz} = \frac{1}{b}\int_0^b y\sigma_{xx}\,\mathrm{d}y \tag{3.59}$$

Then the bending modulus B_{11} is determined as

$$\bar{\mu}_{xz} = B_{11}\kappa^{\circ}_{xz} \tag{3.60}$$

In contrast to the displacement boundary conditions used in the determination of the moduli, the applied loading on the surface of the cell provides an alternative in determining the bending modulus. A simple linear function of the normal stress is applied at $x = a$ for the quarter of the cell as follows

$$\sigma_{xx}(a,y) = 3y/b^2, \quad \sigma_{xy}(a,y) = 0 \tag{3.61}$$

$$\sigma_{yy}(x,b) = 0, \quad \sigma_{xy}(x,b) = 0 \tag{3.62}$$

Using (3.61) and (3.62) and the interface continuity conditions (3.56) and (3.57) with the least squares method, the series solutions can be obtained.

The couple stress is obtained as

$$\bar{\mu}_{xz} = \frac{1}{b}\int_0^b y\sigma_{xx}\,\mathrm{d}y = 1 \tag{3.63}$$

The curvature can be obtained by

$$\bar{\kappa}_{xz} = \frac{1}{2ab}\int_0^b \frac{\partial v(a,y)}{\partial x}\,\mathrm{d}y - \frac{u(a,b)}{2ab} \tag{3.64}$$

where

$$\frac{\partial v}{\partial x} = \cos\theta\left(\sin\theta\frac{\partial u_r}{\partial r} + \cos\theta\frac{\partial u_\theta}{\partial r}\right) - \frac{\sin\theta}{r}\left(\frac{\partial u_r}{\partial\theta}\sin\theta + \frac{\partial u_\theta}{\partial\theta}\cos\theta + u_r\cos\theta - u_\theta\sin\theta\right)$$

where $v = u_r\sin\theta + u_\theta\cos\theta$.

The bending modulus is defined as

$$B_{11} = \frac{1}{\bar{\kappa}_{xz}}$$

4. Results and discussion

The application of classical elasticity theory and micro-polar theory in predicting the micro-stress fields from macro-stress fields near the high macro-gradient zone of the free edge problem in composite laminates will be presented in detail. The composite consist of Sigma 1240 (silicon carbide) fibers (Young's modulus: 325 GPa and Poisson's ratio: 0.15) and epoxy matrix (Young's modulus: 3.45 GPa and Poisson' ratio: 0.35). Two composite laminates are used to critically examine and compare the stress solutions from these two theories with "exact" solutions. 30.7% and 61.4% V_f fibrous unit cells are utilized to construct two composite laminate models. The homogenization method to compute the effective moduli for the two theories of these composite cells has been derived in Yuan et al. (1997) and Section 3. The obtained effective elastic moduli are listed in Table 1(panels a and b). The bending moduli are also obtained from the displacement and stress boundary conditions utilizing the boundary least squares method (Hulbert and Rybicki, 1971) as well as the finite element method as discussed in Section 3. By applying the displacement and stress boundary conditions, a larger discrepancy of B as indicated in Fig. 6 is evident when a higher fiber volume fraction is applied. These moduli based on displacement boundary conditions are then employed in the analysis of the composite laminates.

Table 1
Effective moduli of 30.7% V_f fibrous cell (panel a) and 61.4% V_f fibrous cell (panel b)

Panel a

$E_L = 102.11$ GPa, $E_T = E_Z = 7.27$ GPa, $v_{LT} = v_{LZ} = 0.277$, $v_{TZ} = 0.440$, $G_{LT} = G_{LZ} = 2.39$ GPa, $G_{TZ} = 1.99$ GPa

The micro-polar shear and bending moduli are shown in the constitutive relations

$$\begin{Bmatrix}\bar{\sigma}_{xy}\\ \bar{\sigma}_{yx}\end{Bmatrix} = \begin{bmatrix}22.51 & -18.53\\ -18.53 & 22.51\end{bmatrix}\begin{Bmatrix}\bar{\varepsilon}_{xy}\\ \bar{\varepsilon}_{yx}\end{Bmatrix}\ \text{GPa},\quad \begin{Bmatrix}\bar{\mu}_{xz}\\ \bar{\mu}_{yz}\end{Bmatrix} = \begin{bmatrix}9.53 & 0\\ 0 & 9.53\end{bmatrix}\begin{Bmatrix}\bar{\kappa}_{xz}\\ \bar{\kappa}_{yz}\end{Bmatrix}\ \text{N/m}$$

Panel b

$E_L = 198.99$ GPa, $E_T = E_Z = 14.95$ GPa, $v_{LT} = v_{LZ} = 0.172$, $v_{TZ} = 0.535$, $G_{LT} = G_{LZ} = 5.74$ GPa, $G_{TZ} = 1.87$ GPa

The micro-polar shear and bending moduli are shown in the constitutive relations

$$\begin{Bmatrix}\bar{\sigma}_{xy}\\ \bar{\sigma}_{yx}\end{Bmatrix} = \begin{bmatrix}28.57 & -21.12\\ -21.12 & 28.57\end{bmatrix}\begin{Bmatrix}\bar{\varepsilon}_{xy}\\ \bar{\varepsilon}_{yx}\end{Bmatrix}\ \text{GPa},\quad \begin{Bmatrix}\bar{\mu}_{xz}\\ \bar{\mu}_{yz}\end{Bmatrix} = \begin{bmatrix}17.75 & 0\\ 0 & 17.75\end{bmatrix}\begin{Bmatrix}\bar{\kappa}_{xz}\\ \bar{\kappa}_{yz}\end{Bmatrix}\ \text{N/m}$$

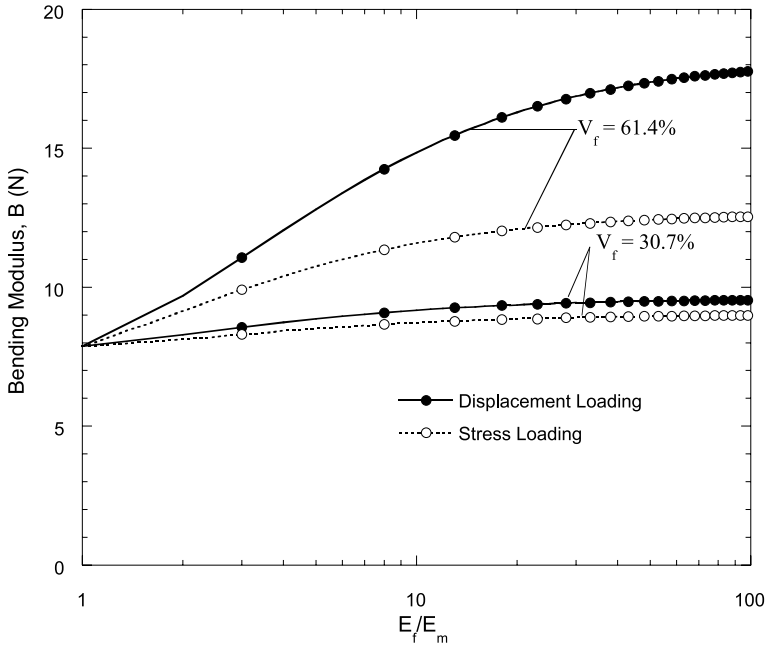

Fig. 6. Bending modulus of 30.7% and 61.4% fiber volume fraction (V_f).

The MM which models the fibers explicitly in the finite element method will serve as "exact" solutions for the laminates within the bounds of the FEM analysis. The stress fields based on EM from classical elasticity theory and MP from micro-polar theory are evaluated and compared with the "exact" solutions. Note that in these two composites the ply interfaces are truly matrix material, but the effective modulus representation (EM and MP models) leads to artificial results—caused by the "discontinuity" in moduli at the interface in the model. The "layered" composites create a high macro-stress gradient near the free edge. The only way to improve the results is to represent the micro-structure explicitly (MM model). Also in the MP model, the couple stress traction vector must vanish on the interface with a classical epoxy matrix. Special attention is focused on the normal stress along artificial interface, $y = h$, and micro-stress along fiber/matrix interface of the critical cell near the high macro-stress gradient region. These micro-stresses are crucial since failure of the composites most likely will initiate along the fiber/matrix interface. It has been demonstrated that the effective modulus model (EM) is not able to capture these micro-stresses accurately (Pagano and Yuan, 2000). The proposed micro-polar theory (MP), which includes a couple stress and an independent rotation in addition to the conventional stresses and displacements of elasticity theory, respectively, may predict these micro-stresses precisely.

4.1. Stress fields near the free edge

The use of micro-polar theory aims at improving prediction of the stress fields near the free edge in the analysis of composite laminates. The region near the free edge is extremely critical due to its steep macro-stress gradient and its physical significance with regard to the failure initiation. Two laminates having the identical macro-geometry and constituents as seen in Figs. 2 and 3 of two-row composite lamina and yet one with 30.7% V_f and the other with 61.4% V_f, under $\varepsilon_z = 0.2\%$ are used for illustration and discussed in the order of increasing stress singularity. The first case, as seen in Fig. 2, is a laminate system that has stress singularity $\delta = -0.0370642$ calculated from the classical elasticity theory. The stress singularity is obtained

by satisfying the "interfacial" continuity at $y = h$ and traction free conditions along the free edge, $x = 4h$. The second case as shown in Fig. 3 with higher fiber volume fraction has stress singularity $\delta = -0.1188763$. Emphasis of the study focuses on the stress fields on planes $y = 0$, $y = h$, $x = 3h$, $x = 4h$ and particularly along the boundary of a unit cell near the free edge where the maximum normal stress occurs; this cell is called a "critical" cell. The stress fields from MM, EM and MP models along the boundary of the critical cell are discussed.

The effects of fiber volume fraction on the stress fields are investigated first. As observed in Fig. 7, the MM normal stress at $y = h$ oscillates due to presence of the fibers. For the case of 30.7% V_f, the EM model gives a distortion of physics since the singular stress is tensile at the edge ($x = 4h$), while the MM (actual) stress is compressive. As expected, when the fiber volume fraction increases, the magnitude of micro-stress increases and macro-stress gradient near the free edge is greater. At the center line $x = 0$, the EM stress for 61.4% V_f case approach a plateau non-zero value which is greater than that of 30.7% V_f case. The non-zero value of σ_y at the center line is manifested by the balance the force and moment along the interface $y = h$. For wider laminates, it is expected that σ_y should approach zero which is consistent with the classical lamination theory.

The normal stress distribution of the first case at $y = 0$ is shown in Fig. 8. The exact average of the stress using MM model generally lies close to the EM and MP curves, except the nearest cell to the free edge. In Fig. 8, MM, EM and MP curves are very close to each other. However, results from the theories shown Fig. 9 give totally different trends at the artificial interface $y = h$ in comparison with those at the plane $y = 0$. In addition, the normal stress distribution of the MP model is slightly different from that of the EM model, especially near the free edge. The comparison of Figs. 8 and 9 suggests that the influence of a particular fiber is only felt within a region of dimension h (cell size), which illustrates "micro-zone of influence" in the lamina. The presence of the free edge creates high macro-stress gradient within each laminate. To illustrate this point, the EM and MP models in Fig. 10 show high σ_y gradient at $y = 160$ μm where an artificial material discontinuity occurs. The implementation of micro-polar theory in the analysis does not significantly

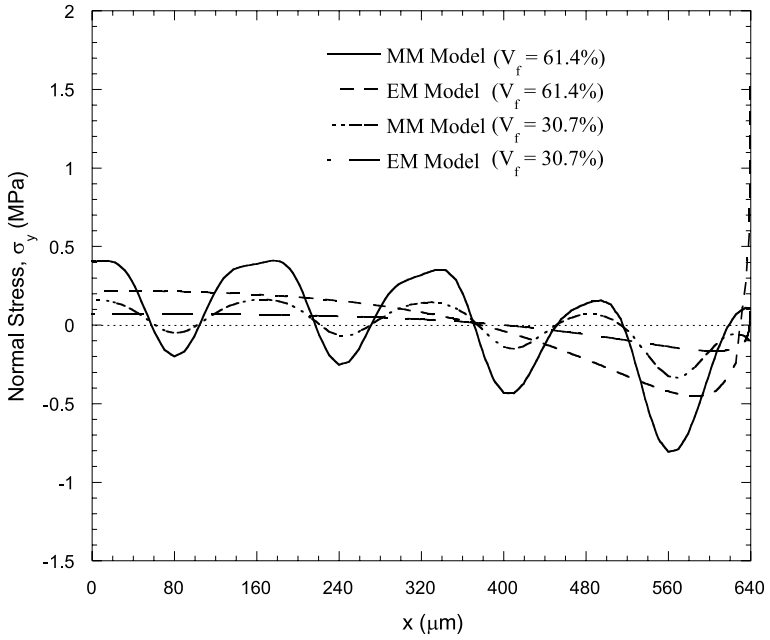

Fig. 7. Effect of volume fraction on σ_y of composite laminate.

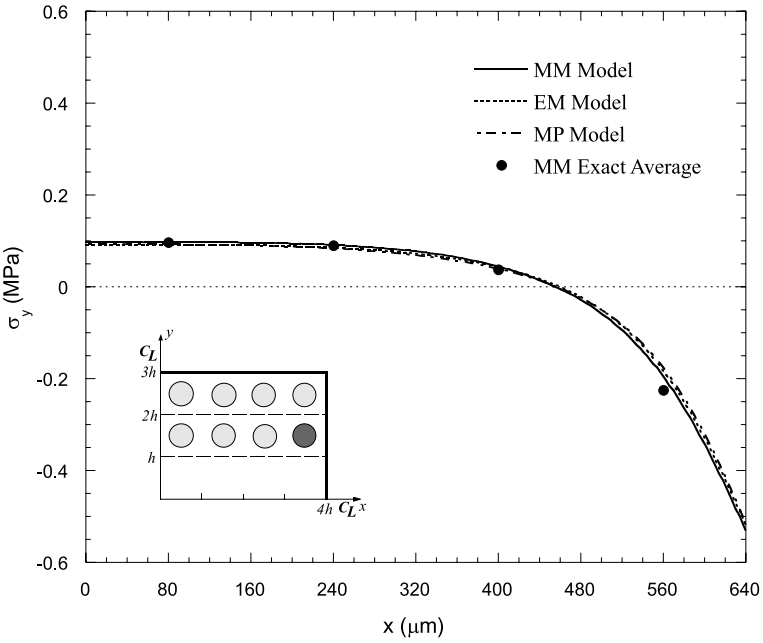

Fig. 8. Case 1: σ_y distribution at $y = 0$.

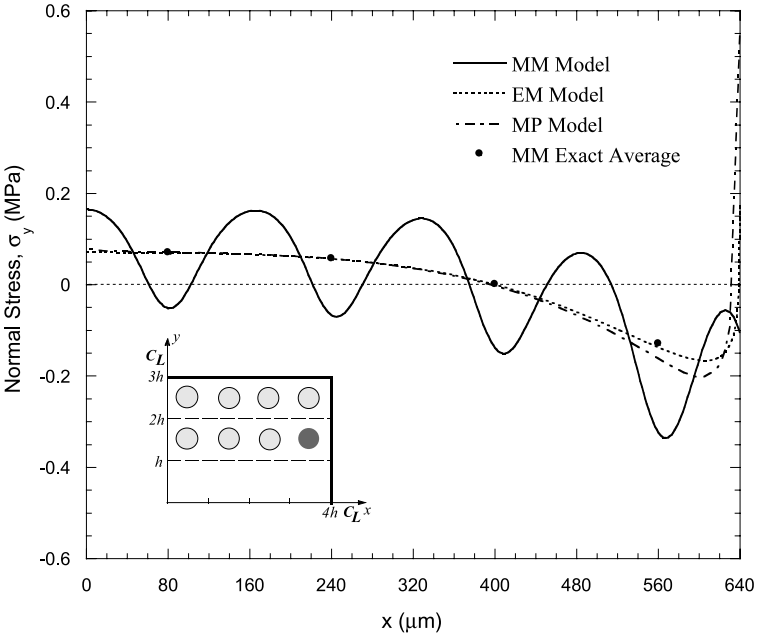

Fig. 9. Case 1: σ_y distribution at $y = h$.

change the stress pattern. Another important observation is the location of the maximum tensile stress in the laminate as demonstrated in Fig. 10. The MM maximum tensile stress falls at $y = (3/2)h$ (240 μm)

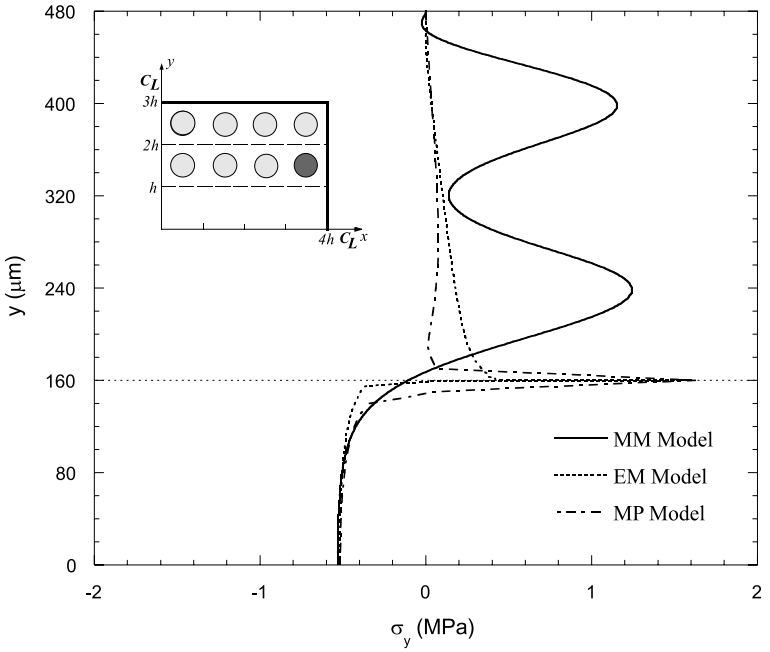

Fig. 10. Case 1: σ_y distribution at $x = 4h$.

whereas the MP and EM maximum tensile stresses take place along the artificial interface. The cell where maximum EM and MP tensile stress exists is identified is the central point of the investigation due to the possible location of failure initiation.

From the results demonstrated in Figs. 8–10, problems are encountered in interpreting regions of steep gradients in the effective modulus solution at $y = h$ and the region along the free edge, $x = 4h$. The discontinuity of elastic moduli in the effective modulus model produces a singularity along planes $x = 4h$ and $y = h$. Obviously, the singularity is an artifact in this case since no material discontinuity exists along the plane $y = h$ in the actual configuration. This fact forces us to examine the meaning of such a wildly variable effective modulus stress field and to question the legitimacy of characterizing the behavior in this region by an average state of stress in the study of a physical phenomenon. In Fig. 9, σ_y is tensile for both EM and MP models hence these models would be expected to predict free edge failure at the interface $y = h$. On the other hand, σ_y of MM model is compressive which means the laminate is not susceptible to free edge failure in the neighborhood of $(4h, h)$. The inconsistency in predicting the normal stress implies that the effective moduli approach needs careful interpretation with regard to the prediction of physical behavior in the present class of problems, as well as in other problems in which a stress singularity exists.

In order to assess if the effective modulus theory represents reasonable stress field predictions of the micro-mechanics model, the comparison of the resultant stresses around the boundary of the critical cell is evaluated and listed in Table 2. A strong indication of the improved stress predictions from the MP model is demonstrated. Notice that the resultant shear stress is anti-symmetric, hence, the unit cell is now subjected to both resultant stresses and moments. The total moment from MP model is computed by the combination of moment resulting from the normal stresses and couple stress of micro-polar theory. Overall, good agreement is achieved between the MM and MP models. While the EM and MP models may produce irregularity in the stress field prediction, the MP resultant stresses compare quite well with those given by the "exact" analysis (MM model). After evaluating the boundary of the critical cell, one can conclude that

Table 2
Case 1: Resultant stresses on the 'critical' cell

MM (micro-mechanics model)

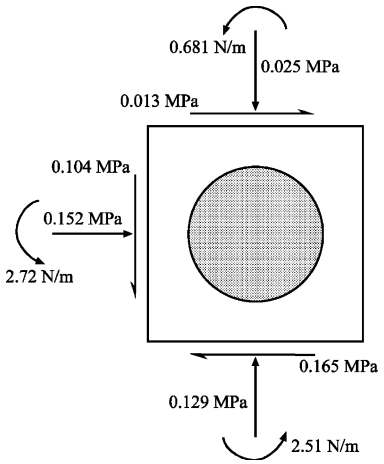

EM (effective modulus model)

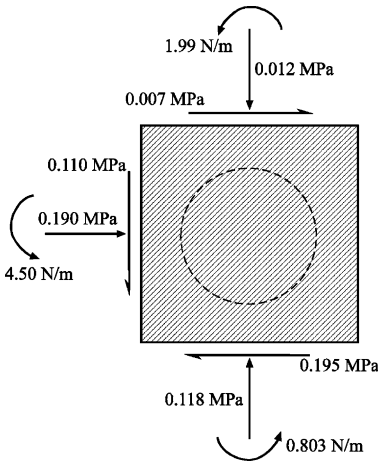

MP (micro-polar model)

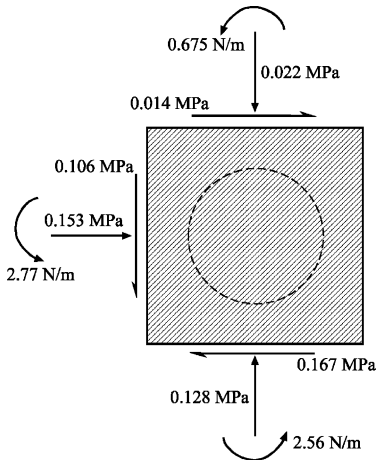

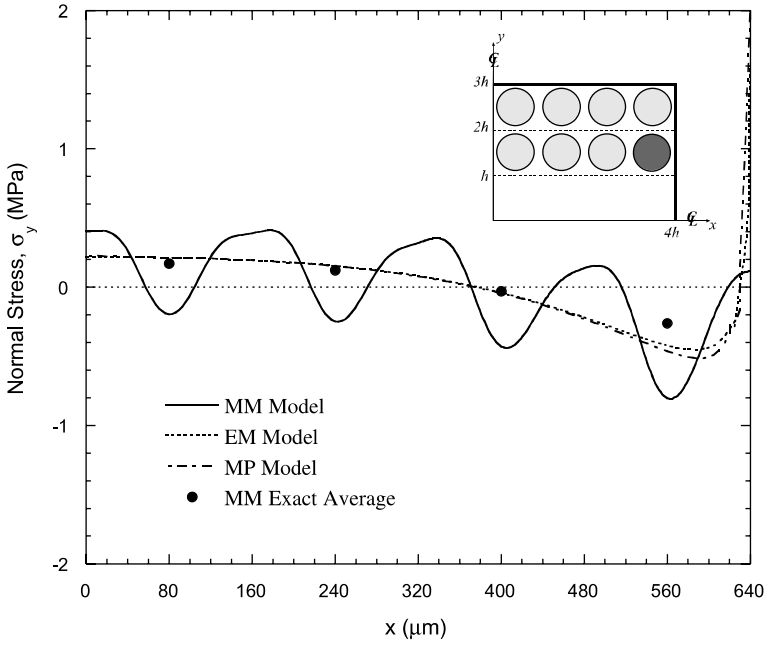

Fig. 11. Case 2: σ_y distribution at $y = h$.

the micro-polar theory significantly improves the prediction of resultant stresses near the free edge of the composite laminate.

A similar analysis is applied to composite laminate consisting of 61.4% V_f cells. It can be observed in Fig. 11 that the magnitude of the normal stress, in general, increases as the fiber volume fraction increases. The MP model also gives a similar high macro-stress gradient as the EM model as indicated in Fig. 12. In addition, as in the first case, EM model using 61.4% V_f cells fails to provide accurate predictions of the resultant stress on the critical cell as clearly seen in Table 3. However, the MP model successfully predicts these stresses, although it is not as accurate as the results in low fiber volume fraction case, such as in the first case.

In summary, the complex behavior of the composite laminates, particularly the physical meaning of the normal stresses is very difficult to interpret. From the ply level, EM stresses can be physically deceptive, i.e., can lead to unreasonable prediction of failure initiation. Failure, here, is interpreted as a crack to initiate at the free edge and then propagate into the matrix region. However, in the micro-level, the stresses along the fiber/matrix interface, so called micro-stress, are expected to dominate laminate failure. Thus, the need to implement micro-polar theory in the micro-stress prediction of "critical" cell is more apparent to confidently determine the failure criteria of composite laminates. The micro-stresses in all cases considered above are examined along fiber/matrix interface in the following section.

4.2. Micro-stresses at fiber/matrix interface

Micro-mechanical stresses affect the strength of fiber reinforced composites. In addition, initial cracking in composites usually occurs in the matrix or the interface between fiber and matrix. Therefore, the most important part in the design analysis of composite lamina, especially in the failure analysis of composites is the stress distribution along fiber/matrix interface. For the present boundary value problem, the implementation

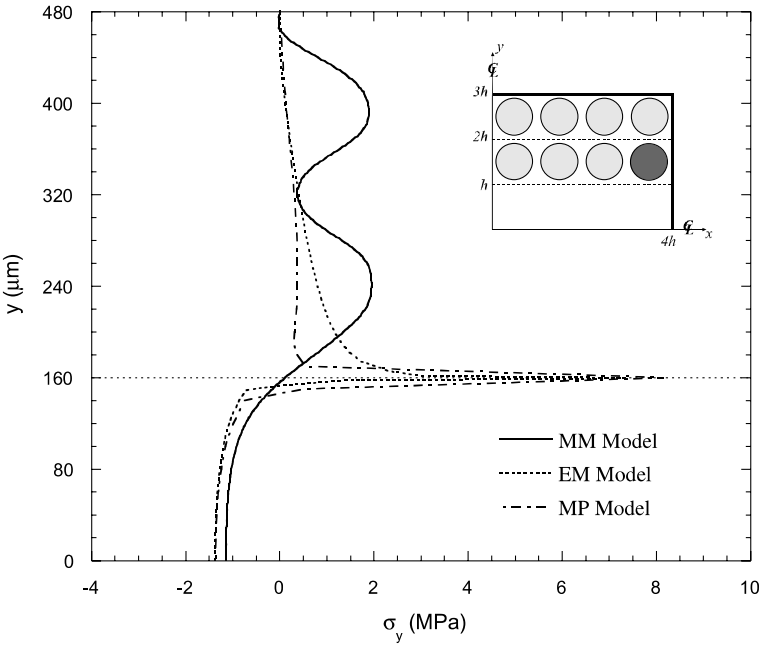

Fig. 12. Case 2: σ_y distribution at $x = 4h$.

of micro-polar theory into composite laminate mechanics appears to be beneficial in predicting these micro-stress. To demonstrate this point, nodal forces attained from the boundary of the critical cell are applied to a unit cell. For MP model, in addition to the direct nodal forces, the nodal force due to the couple stress is also implemented to the computation scheme around the boundary of the critical cell. The micro-stress from MM, EM and MP models are then compared.

The micro-stress prediction of the first case obtained from traction boundary conditions are plotted in Fig. 13(a)–(d). The solid lines represent MM micro-stress. In the solid curves of Fig. 13(a) and (d), the distribution of σ_r and $\sigma_{r\theta}$, which, of course are equal in exact elasticity solution but are natural boundary conditions in the FEM. Hence, the proximity of the results (the solid lines are actually two curves) is a sign of the convergence of the FEM solution. In Fig. 13(c), the matrix stress distribution of σ_θ is displayed. The micro-stress σ_θ in the fiber are also presented in Fig. 13(b). The other curves in Fig. 13(a)–(d) represent EM and MP models. In Fig. 13(a)–(d), the EM and MP results are plotted in open diamond and solid circles, respectively. The micro-stress from traction boundary conditions calculated from EM and MP models along the three critical cell boundaries, $y_o = h/2, -h/2$ and $x_o = -h/2$, and traction free boundary at $x_o = h/2$, where x_o, y_o are the center coordinate of the critical fiber, are displayed and compared with the exact MM model. It is shown in Fig. 13(a)–(d) that the micro-stress from the MP model is in very good agreement with the "exact" micro-stress. Fig. 14 shows that micro-polar theory is able to improve greatly the prediction of strain distribution, ε_y, at the free edge of the critical cell.

Lastly, the case with a higher stress singularity model is examined by utilizing 61.4% V_f fibrous cells. The micro-stress obtained from traction boundary conditions applied at the critical cell boundary are plotted. It is observed in Fig. 15(a)–(d), using higher fiber volume fraction, the EM solutions do not provide accurate results in micro-stress prediction. However, MP solutions produce more accurate micro-stress prediction as seen in Fig. 15(a)–(d). MP model also improves the strain, ε_y, distribution at the free edge, as seen in Fig. 16.

Table 3
Case 2: Resultant stresses on the 'critical' cell

MM (micro-mechanics model)	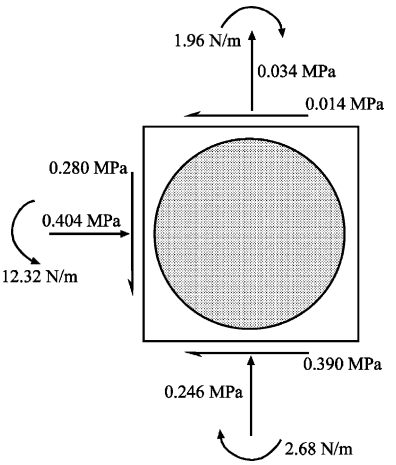
EM (effective modulus model)	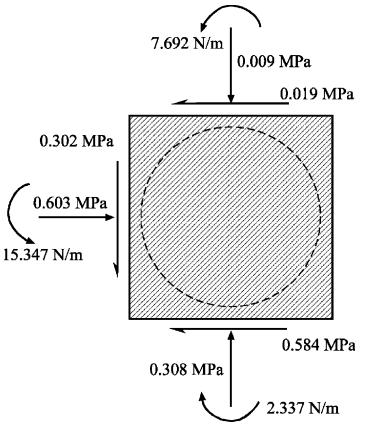
MP (micro-polar model)	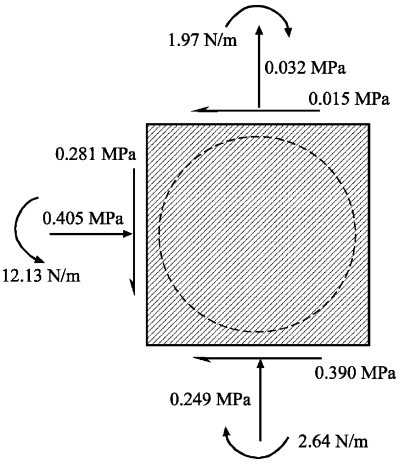

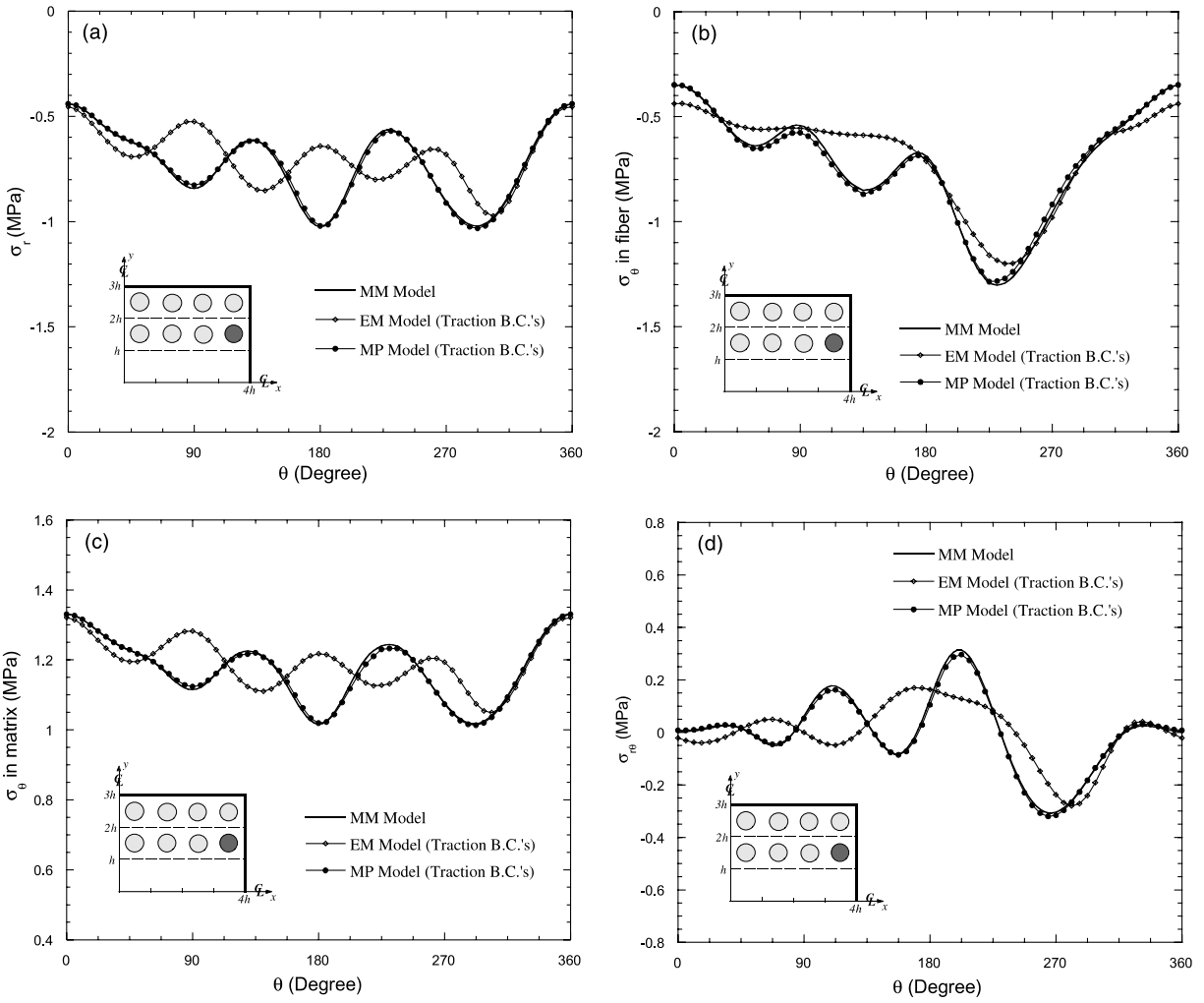

Fig. 13. (a) Case 1: σ_r of the critical cell along the fiber/matrix interface. (b) Case 1: σ_θ in the fiber of the critical cell along the fiber/matrix interface. (c) Case 1: σ_θ in the matrix of the critical cell along the fiber/matrix interface. (d) Case 1: $\sigma_{r\theta}$ of the critical cell along the fiber/matrix interface.

In conclusion, the micro-stress would be expected to dominate the initial failure process due to the maximum stress location in the interfacial zones. Consequently, it is critical to be able to predict the micro-stress along fiber/matrix interface, and the micro-polar theory clearly shows much better prediction of these stresses.

5. Conclusions

The micro-polar homogenization is used to predict the micro-stress distribution in the region of high macro-stress gradient of the composite laminates. The higher-order elasticity theory is based on the micro-

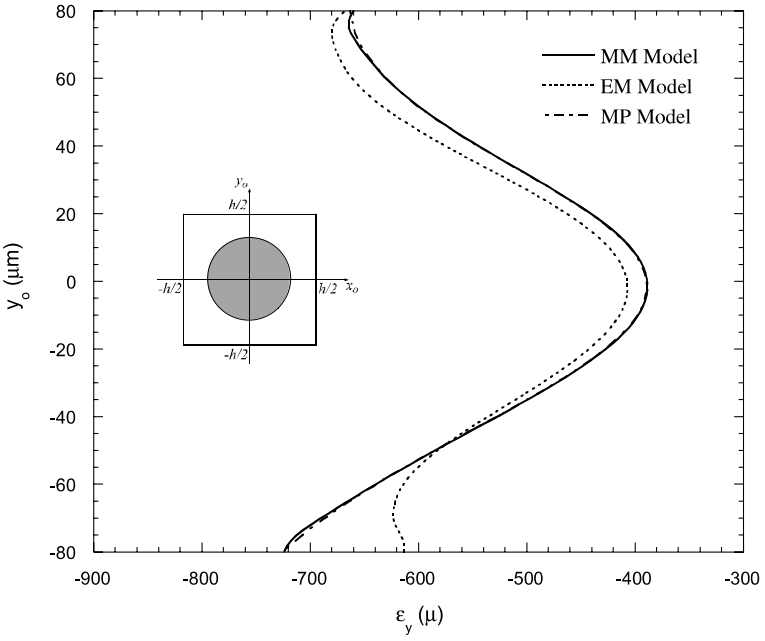

Fig. 14. Case 1: ε_y of the critical cell along $x_o = h/2$.

polar theory developed by Eringen (1966). The in-plane shear moduli and the bending moduli are determined from a nine-cell model and a long strip of unit cells respectively. In order to substantiate its applicability, two cases of laminates with free edge under uniform axial strain have been studied. The following conclusions may be drawn:

(1) The micro-polar homogenization method is introduced to determine the effective moduli of composite materials by means of the finite element method. In addition to the classical effective moduli, the micro-polar shear and bending moduli are utilized to introduce the cell size factor that exists in micro-polar theory.

(2) In the classical elasticity theory, the fiber volume fraction and the cell size affect the stress response of the composite laminate. First, in the class of problems studied there is inconsistency in predicting the normal stress, especially at the free edge when 30.7% and 61.4% V_f cell laminates are employed. For the case of 30.7% V_f, the EM model gives a distortion of physics since the singular stress is tensile at the free edge while the MM stress is compressive. Second, a strong indication of a 'micro-zone of influence' around the boundary of the cell near the free edge is observed. The term 'micro-zone of influence' implies that the stress and strain distributions around the boundary of the cell vary with the cell size (fiber size). A 'Micro-zone of influence' can also be interpreted as the influence of a particular fiber is only felt within a region of fiber size (dimension h). Due to the importance of the cell size on predicting the elastic response of composite laminates, the micro-polar theory which takes into account the cell size or dimension is studied.

(3) Similar to the classical elasticity theory, the application of micro-polar theory to composite laminate introduces artificial interfaces leading to severe macro-stress gradient, which can distort the physics of the problem by reversing the sign of the normal stress near the free edge region. The inconsistency in predicting the normal stress at the artificial interface implies that the effective moduli approach, the classical and micro-polar elasticity theory, needs careful interpretation with regard to the prediction of physical behavior in the present problem, as well as in other problems in which effective singularities exist. The advantage of the micro-polar theory can be clearly seen by evaluating the resultant stresses on the boundary of the

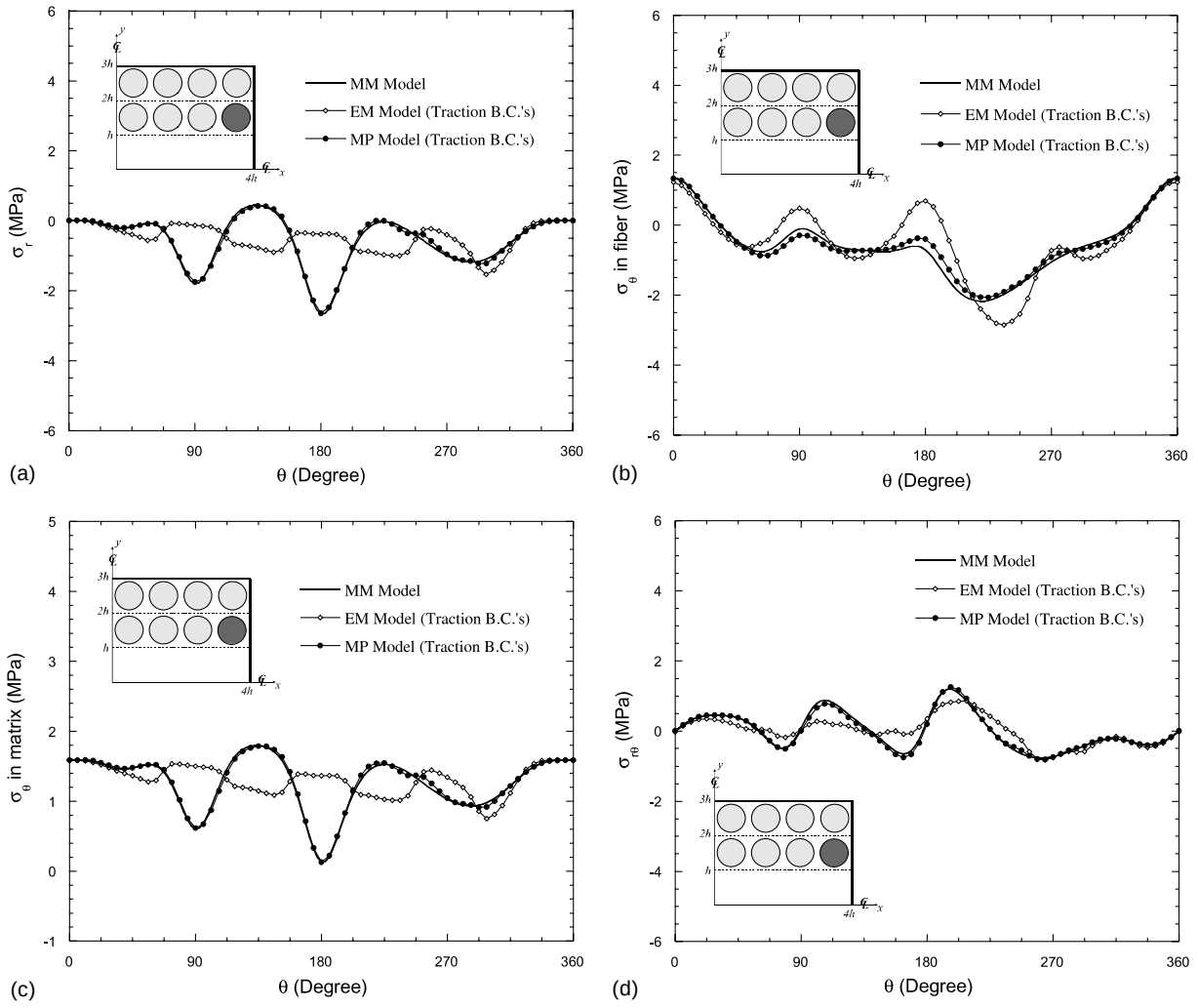

Fig. 15. (a) Case 2: σ_r of the critical cell along the fiber/matrix interface. (b) Case 2: σ_θ in the fiber of the critical cell along the fiber/matrix interface. (c) Case 2: σ_θ in the matrix of the critical cell along the fiber/matrix interface. (d) Case 2: $\sigma_{r\theta}$ of the critical cell along the fiber/matrix interface.

critical cell, near the free edge of the composite laminate. It is clear that the classical effective modulus theory (EM model) is not able to predict these stresses, while the micro-polar theory produces accurate prediction of the resultant stresses.

(4) The micro-stress predictions near the steep macro-stress gradient using micro-polar theory from the ply level for all cases are very promising although the micro-polar theory only considers the gradient of the normal stress (couple stress) but not shear stress. These microstresses are responsible for the failure initiation process in composites since the composite failure always originates from the micro-scale. In general, the micro-polar theory improves the micro-stress predictions using both displacement and traction boundary conditions imposed on the critical cell boundaries. However, the use of displacement boundary conditions in the laminate with higher fiber volume fraction, such as in the second case, is not able to

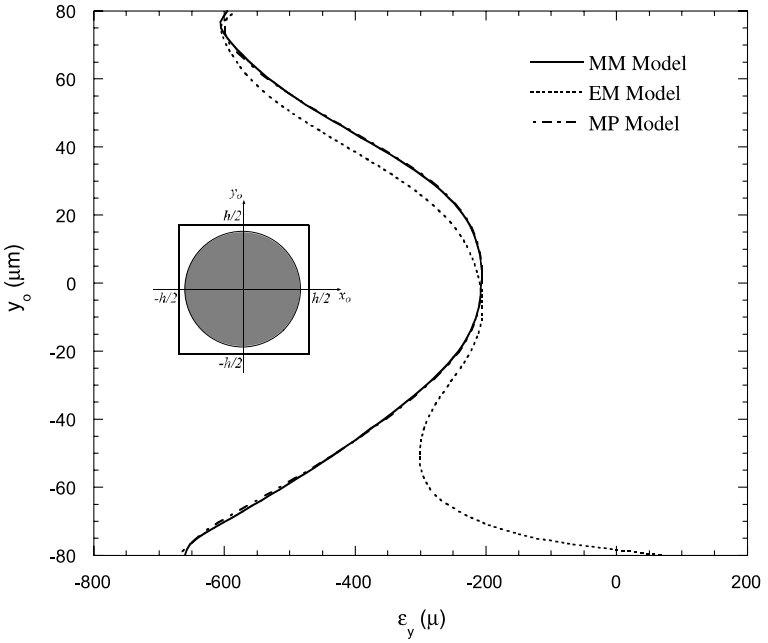

Fig. 16. Case 2: ε_y of the critical cell along $x_o = h/2$.

capture or even provide similar micro-stress trends as in the "exact" solutions (MM model). Note that the independent rotation has not been taken into account in the displacement boundary conditions along the cell boundary. It is hopeful that the inclusion of this rotation in the boundary condition will further improve the micro-stress prediction.

(5) The micro-polar theory may be used to establish realistic failure criteria for composite laminates in the presence of stress concentrations and steep stress gradients at the micro-mechanical scale.

Acknowledgement

This research is supported by the Air Force Office of Scientific Research under grant no. F49620-99-1-0110.

Appendix A. Finite element method for micro-polar elasticity

The principle of virtual work and the variational principle of total potential energy for micro-polar elastic materials will be derived in this section. A general three-dimensional finite element method is formulated. A finite element scheme is examined under two-dimensional general plane deformation subjected to uniaxial strain. An example is shown for the infinite strip under in-plane shear for which an exact solution is known. Solution of the example is compared with those from the finite element method to show the accuracy of this method.

A.1. Principle of virtual work and variational formulation of micro-polar elasticity

The micro-polar theory incorporates independent micro-rotations as well as the translational displacements assumed in classical elasticity. The principle of virtual work can be obtained from the equations of equilibrium and vice versa. Let a solid body in V be in static equilibrium under specified body forces, body couples, and surface boundary conditions. The surface boundary of the body S can be divided into two parts from the viewpoint of the boundary conditions. The part S_σ over which traction boundary conditions are prescribed in terms of external forces and couples and the part S_u over which geometrical boundary conditions are prescribed in terms of displacements and micro-rotations. Thus, $S = S_\sigma + S_u$. Here, the arbitrary set of the virtual displacements is chosen such that the geometrical boundary conditions on S_u satisfy the following equations:

$$\delta\boldsymbol{u} = [\delta u, \delta v, \delta w]^{\mathrm{T}} = 0 \quad \text{and} \quad \delta\boldsymbol{\phi} = [\delta\phi_x, \delta\phi_y, \delta\phi_z]^{\mathrm{T}} = 0, \quad \text{on } S_u \tag{A.1}$$

The stress components are denoted by $\sigma_x, \sigma_y, \ldots, \sigma_{xy}$ and couple-stresses by $\mu_{xx}, \mu_{yy}, \ldots, \mu_{xy}$. Equilibrium equations in the absence of body forces and body couples at all points in V are expressed by:

$$\sigma_{ji,j} = 0, \quad \mu_{ji,j} + \varepsilon_{ikl}\sigma_{kl} = 0 \tag{A.2a,b}$$

The traction boundary conditions are given by

$$t_i^{(n)} = \bar{t}_i^{(n)}, \quad \mu_i^{(n)} = \bar{\mu}_i^{(n)} \quad \text{on } S_\sigma \tag{A.3a,b}$$

Multiplying Eq. (A.2a,b) by the arbitrary virtual displacements $\delta\boldsymbol{u}$ and $\delta\boldsymbol{\phi}$, respectively and integrating the relation over V, multiplying Eq. (A.3a,b) by the virtual displacements and integrating over S_σ, and then applying Gauss' theorem the sum of the two integrals leads to

$$\int_V [\sigma_{ji}\delta u_{i,j} + \mu_{ji}\delta\phi_{i,j} - \varepsilon_{ikl}\sigma_{kl}\delta\phi_i]\,\mathrm{d}V - \int_{S_\sigma} (\bar{t}_i^{(n)}\delta u_i + \bar{\mu}_i^{(n)}\delta\phi_i)\,\mathrm{d}S = 0 \tag{A.4}$$

By introducing the micro-polar strain tensor

$$\varepsilon_{ij} = u_{j,i} - \varepsilon_{ijk}\phi_k \tag{A.5}$$

Eq. (A.4) can be rewritten as

$$\int_V (\sigma_{ij}\delta\varepsilon_{ij} + \mu_{ji}\delta\phi_{i,j})\,\mathrm{d}V - \int_{S_\sigma} (\bar{t}_i^{(n)}\delta u_i + \bar{\mu}_i^{(n)}\delta\phi_i)\,\mathrm{d}S = 0 \tag{A.6}$$

The integrals can be recognized as work expressions. The first integral corresponds to the negative of the internal virtual work and the second integral is the virtual external work. Hence

$$-\delta W_i - \delta W_e = 0 \tag{A.7}$$

This expression can be expressed by

$$\delta(W_i + W_e) = 0 \quad \text{or } \delta W = 0 \tag{A.8}$$

with

$$W = W_i + W_e$$

Eqs. (A.6) and (A.7) or (A.8) are the expressions for the principle of virtual work. The principle holds for arbitrary infinitesimal virtual displacements satisfying the prescribed geometrical boundary conditions.

For dissipation-free materials and conservative loads, we assume the existence of a positive definite strain energy density $U_0(\varepsilon_{ij}, \kappa_{ij})$ such that

$$\sigma_{ij} = \frac{\partial U_0}{\partial \varepsilon_{ij}} \quad \text{and} \quad \mu_{ij} = \frac{\partial U_0}{\partial \kappa_{ij}} \tag{A.9}$$

where

$$\kappa_{ij} = \phi_{j,i} \tag{A.10}$$

Then, the first term of Eq. (A.6) is expressed by

$$\int_V \left[\frac{\partial U_0}{\partial \varepsilon_{ij}} \delta\varepsilon_{ij} + \frac{\partial U_0}{\partial \kappa_{ij}} \delta\kappa_{ij} \right] \mathrm{d}V = \delta \int_V U_0 \, \mathrm{d}V = \delta U \tag{A.11}$$

The virtual work of the external loads may be expressed in terms of the variation of the load potential as

$$\delta W_e = \int_{S_\sigma} (\bar{t}_i^{(n)} \delta u_i + \bar{\mu}_i^{(n)} \delta\phi_i) \, \mathrm{d}S = \delta \int_{S_\sigma} (\bar{t}_i^{(n)} u_i + \bar{\mu}_i^{(n)} \phi_i) \, \mathrm{d}S = -\delta V \tag{A.12}$$

Eq. (A.6) can be written as

$$\delta U + \delta V = 0 \tag{A.13}$$

Total potential energy is defined as

$$\Pi = U + V \tag{A.14}$$

Now, Eq. (A.12) can be expressed as

$$\delta\Pi = 0 \tag{A.15}$$

Eq. (A.15) is the principle of total potential energy of micro-polar elasticity in which strain energy and the potential of the external load are given by Eqs. (A.11) and (A.12), respectively.

A.2. FEM under generalized plane deformation

For generalized plane deformation problem to be discussed later where the displacements and rotation are expressed by

$$\begin{aligned} u(x,y,z) &= U(x,y) \\ v(x,y,z) &= V(x,y) \\ w(x,y,z) &= \varepsilon_0 z \\ \phi_z(x,y,z) &= \phi_z(x,y) \end{aligned} \tag{A.16}$$

and stresses are functions of x and y only, the three-dimensional constitutive equations can be significantly simplified.

$$\begin{Bmatrix} \sigma_{xx} \\ \sigma_{yy} \\ \sigma_{xy} \\ \sigma_{yx} \\ \mu_{xz} \\ \mu_{yz} \end{Bmatrix} = \begin{bmatrix} C_{11} & C_{12} & 0 & 0 & 0 & 0 \\ C_{21} & C_{22} & 0 & 0 & 0 & 0 \\ 0 & 0 & G_{11} & G_{12} & 0 & 0 \\ 0 & 0 & G_{12} & G_{22} & 0 & 0 \\ 0 & 0 & 0 & 0 & B_{11} & B_{12} \\ 0 & 0 & 0 & 0 & B_{12} & B_{22} \end{bmatrix} \begin{Bmatrix} \varepsilon_{xx} \\ \varepsilon_{yy} \\ \varepsilon_{xy} \\ \varepsilon_{yx} \\ \kappa_{xz} \\ \kappa_{yz} \end{Bmatrix} + \begin{Bmatrix} C_{13} \\ C_{23} \\ 0 \\ 0 \\ 0 \\ 0 \end{Bmatrix} \varepsilon_0 \tag{A.17}$$

or

$$\begin{aligned}
&\boldsymbol{\sigma} = \boldsymbol{D}\boldsymbol{\varepsilon} + \boldsymbol{\sigma}_0 \\
&\boldsymbol{\sigma} = [\sigma_{xx}, \sigma_{yy}, \sigma_{xy}, \sigma_{yx}, \mu_{xz}, \mu_{yz}]^{\mathrm{T}} \\
&\boldsymbol{\varepsilon} = [\varepsilon_{xx}, \varepsilon_{yy}, \varepsilon_{xy}, \varepsilon_{yx}, \kappa_{xy}, \kappa_{yx}]^{\mathrm{T}} \\
&\boldsymbol{u} = [u, v, \phi_z]^{\mathrm{T}}
\end{aligned} \tag{A.18}$$

The total potential energy can be expressed by

$$\Pi = \frac{1}{2}\int_V \boldsymbol{\varepsilon}^{\mathrm{T}}\boldsymbol{D}\boldsymbol{\varepsilon}\,\mathrm{d}V + \frac{1}{2}\int_V \boldsymbol{\sigma}_0^{\mathrm{T}}\boldsymbol{\varepsilon}\,\mathrm{d}V \tag{A.19}$$

The strains are given by

$$\boldsymbol{\varepsilon} = \begin{Bmatrix} \varepsilon_{xx} \\ \varepsilon_{yy} \\ \varepsilon_{xy} \\ \varepsilon_{yx} \\ \kappa_{xz} \\ \kappa_{yz} \end{Bmatrix} = \begin{bmatrix} \dfrac{\partial}{\partial x} & 0 & 0 \\ 0 & \dfrac{\partial}{\partial y} & 0 \\ 0 & \dfrac{\partial}{\partial x} & -1 \\ \dfrac{\partial}{\partial y} & 0 & 1 \\ 0 & 0 & \dfrac{\partial}{\partial x} \\ 0 & \dfrac{\partial}{\partial y} & 0 \end{bmatrix} \begin{Bmatrix} u \\ v \\ \phi_z \end{Bmatrix} \tag{A.20}$$

In a finite element representation the displacements and local rotations may be expressed by introducing appropriate shape functions $\boldsymbol{N}$ such that

$$\boldsymbol{u} = \boldsymbol{N}\boldsymbol{u}^e \tag{A.21}$$

where $\boldsymbol{u}^e$ are nodal field variable vectors.

Applying Eq. (A.21) to (A.20) yields

$$\boldsymbol{\varepsilon} = \begin{Bmatrix} \varepsilon_{xx} \\ \varepsilon_{yy} \\ \varepsilon_{xy} \\ \varepsilon_{yx} \\ \kappa_{xz} \\ \kappa_{yz} \end{Bmatrix} = \begin{bmatrix} \dfrac{\partial N}{\partial x} & 0 & 0 \\ 0 & \dfrac{\partial N}{\partial y} & 0 \\ 0 & \dfrac{\partial N}{\partial x} & -1 \\ \dfrac{\partial N}{\partial y} & 0 & 1 \\ 0 & 0 & \dfrac{\partial N}{\partial x} \\ 0 & \dfrac{\partial N}{\partial y} & 0 \end{bmatrix} \begin{Bmatrix} u^e \\ v^e \\ \phi_z^e \end{Bmatrix} = \boldsymbol{B}\boldsymbol{u}^e \tag{A.22}$$

Eq. (A.19) becomes:

$$\Pi = \frac{1}{2}\boldsymbol{u}^{e^{\mathrm{T}}}\left[\int_V (\boldsymbol{B}^{\mathrm{T}}\boldsymbol{D}\boldsymbol{B})\,\mathrm{d}V\right]\boldsymbol{u}^e + \frac{1}{2}\int_V \boldsymbol{\sigma}_0^{\mathrm{T}}\boldsymbol{B}\,\mathrm{d}V\boldsymbol{u}^e \tag{A.23}$$

Taking the first variation of Eq. (A.23) with respect to $\boldsymbol{u}^e$ and a general matrix formulation can be written as:

$$\boldsymbol{k}^e\boldsymbol{u}^e = \boldsymbol{f}^e \tag{A.24}$$

with

$$\boldsymbol{k}^e = \int_V \boldsymbol{B}^{\mathrm{T}}\boldsymbol{D}\boldsymbol{B}\,\mathrm{d}V \tag{A.25}$$

$$\boldsymbol{f}^e = -\int_V \boldsymbol{\sigma}_0^{\mathrm{T}}\boldsymbol{B}\,\mathrm{d}V \tag{A.26}$$

A.3. Numerical example—simple shear of infinite layer

Analytical solutions of an infinite layer under simple shear for a linear isotropic micro-polar solid originally derived by Schaefer (1962) are briefly rederived in this section. The finite element results for this boundary value problem will then be compared with the analytical results to demonstrate the accuracy of the numerical modeling. For an infinite layer in the x-direction under simple shear, the displacements u, ϕ_z, are only a function of y and so do the stress and couple, σ_{xy}, μ_{yz} and $v = 0$. The constitutive relation of a linear isotropic micro-polar solid in plane strain is given by

$$\begin{Bmatrix} \sigma_{xx} \\ \sigma_{yy} \\ \sigma_{xy} \\ \sigma_{yx} \\ \mu_{xz} \\ \mu_{yz} \end{Bmatrix} = \begin{bmatrix} \lambda+2\mu & \lambda & 0 & 0 & 0 & 0 \\ \lambda & \lambda+2\mu & 0 & 0 & 0 & 0 \\ 0 & 0 & \mu+\kappa & \mu-\kappa & 0 & 0 \\ 0 & 0 & \mu-\kappa & \mu+\kappa & 0 & 0 \\ 0 & 0 & 0 & 0 & \gamma & 0 \\ 0 & 0 & 0 & 0 & 0 & \gamma \end{bmatrix} \begin{Bmatrix} \varepsilon_{xx} \\ \varepsilon_{yy} \\ \varepsilon_{xy} \\ \varepsilon_{yx} \\ \kappa_{xz} \\ \kappa_{yz} \end{Bmatrix} \tag{A.27}$$

For this boundary value problem, the constitutive relation can be simply reduced to:

$$\begin{aligned} \sigma_{xy} &= (\mu+\kappa)\varepsilon_{xy} + (\mu-\kappa)\varepsilon_{yx} \\ \sigma_{yx} &= (\mu-\kappa)\varepsilon_{xy} + (\mu+\kappa)\varepsilon_{yx} \end{aligned} \tag{A.28}$$

$$\mu_{yz} = \gamma\kappa_{yz} \tag{A.29}$$

The kinematics relation gives:

$$\varepsilon_{xx} = \varepsilon_{yy} = 0, \quad \varepsilon_{xy} = -\phi_z, \quad \varepsilon_{yx} = \frac{\mathrm{d}u}{\mathrm{d}y} + \phi_z, \quad \kappa_{yz} = \frac{\mathrm{d}\phi_z}{\mathrm{d}y} \tag{A.30}$$

The equations of equilibrium can be reduced to:

$$\frac{\mathrm{d}\sigma_{yx}}{\mathrm{d}y} = 0 \tag{A.31}$$

$$\frac{\mathrm{d}\mu_{yz}}{\mathrm{d}y} + \sigma_{xy} - \sigma_{yx} = 0 \tag{A.32}$$

From Eq. (A.31), σ_{yx} is a constant equal to the applied shear stress on the top and bottom surfaces. Applying Eqs. (A.28)–(A.30) to Eqs. (A.31) and (A.32) and rearranging them, we obtain:

$$\frac{\gamma}{4\kappa}\frac{\mathrm{d}^2\phi_z}{\mathrm{d}y^2} - \phi_z = \frac{1}{2}\frac{\mathrm{d}u}{\mathrm{d}y} \tag{A.33}$$

$$\frac{\gamma(\mu+\kappa)}{2\kappa}\frac{\mathrm{d}^2\phi_z}{\mathrm{d}y^2} - 2\mu\phi_z = \sigma_{yx} \tag{A.34}$$

Further by applying boundary conditions, $\phi_z(\pm h/2) = 0$, we can solve for ϕ_z in the layer from Eq. (A.34)

$$\frac{\phi_z}{\sigma_{yx}} = -\frac{1}{2\mu}\left(1 - \frac{\cosh \xi y}{\cosh \xi h/2}\right) \tag{A.35}$$

where $\xi = 2\sqrt{\frac{\mu\kappa}{\gamma(\mu+\kappa)}}$.

Substituting (A.35) into (A.29), (A.30) and (A.32), then the ratio of the shear stresses can be expressed in the following:

$$\frac{\sigma_{xy}}{\sigma_{yx}} = 1 - \frac{2\kappa}{\mu+\kappa}\frac{\cosh \xi y}{\cosh \xi h/2} \tag{A.36}$$

The couple stress expression can be obtained using (A.29), (A.30) and (A.35).

$$\frac{\mu_{yz}}{\sigma_{yx}} = \frac{1}{2\mu}\xi\frac{\sinh \xi y}{\cosh \xi h/2}$$

The u displacement can be obtained by substituting (A.35) to (A.33) and taking the integration:

$$\frac{u}{\sigma_{yx}} = \frac{1}{\mu}\left[y - \left(\frac{2\mu+\kappa}{\mu+\kappa}\right)\frac{1}{\xi}\frac{\sinh \xi y}{\cosh \xi h/2}\right] \tag{A.37}$$

For numerical illustration, the geometry and relevant material properties are listed:

$$h = 1 \text{ m}, \quad \kappa = 2\mu = 2 \text{ Pa}, \quad \gamma = 1 \text{ N} \tag{A.38}$$

A finite element program based on linear micro-polar theory is tested by applying the equivalent displacement u from Eq. (A.37) at $y = \pm h/2$ with the given boundary conditions $v = \phi_z = 0$ on the surfaces of the infinite layer and utilizing the micro-polar moduli in Eq. (A.38). A two-dimensional analysis with eight-

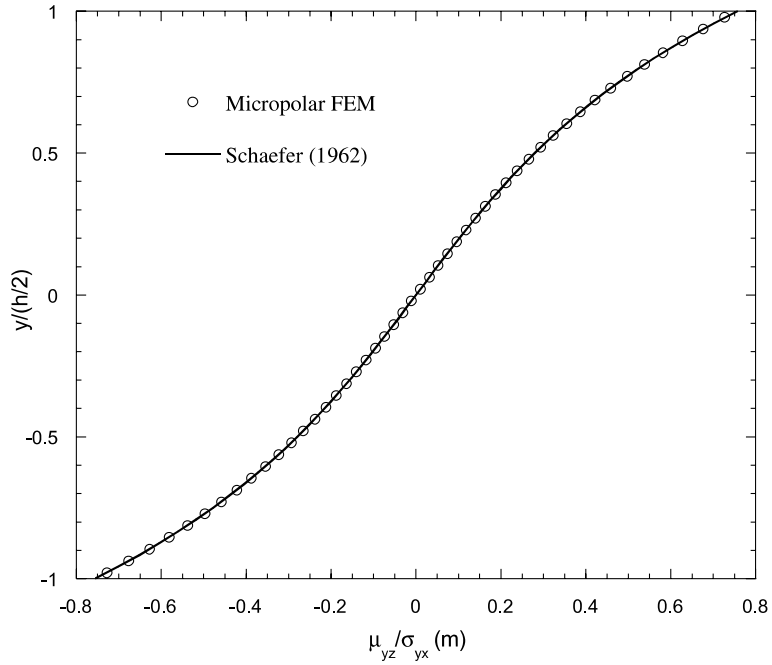

Fig. 17. Couple stress distribution through the thickness of an infinite layer under simple shear.

node isoparametric finite elements is used in the modeling. For example, it is clear from Fig. 17 that finite element results for distributions of μ_{yz} agrees well with the analytical results. Thus, the finite element micropolar program can be confidently employed.

References

Achenbach, J.D., 1973. A theory of elasticity with microstructure for directionally reinforced composites. Springer-Verlag, New York.

Atkinson, C., Leppington, F.G., 1977. The effect of couple stresses on the tip of a crack. Int. J. Solids Struct. 13, 1103–1122.

Bogy, D.B., Sternberg, E., 1968. The effect of couple-stresses on the corner singularity due to an asymmetric shear loading. Int. J. Solids Struct. 4, 159–174.

Chou, T.-W., 1992. Microstructural design of fiber composites. Cambridge University Press, Cambridge.

Cosserat, E., Cosserat, F., 1909. Theorie des corps deformables. A. Herman et Fils, Paris.

Eringen, A.C., 1966. Linear theory of micropolar elasticity. J. Math. Mech. 15, 909–923.

Fish, J., Fares, N., Nath, A., 1993. Micromechanical elastic crack-tip stresses in a fibrous composite. Int. J. Fracture 60, 135–146.

Forest, S., Sab, K., 1998. Cosserat overall modeling of heterogeneous materials. Mech. Res. Commun. 25, 449–454.

Forest, S., 1998. Mechanics of generalized continua: construction by homogenization. J. Physique IV 8, Pr.4-39–Pr.4-48.

Hedgepath, J.M., 1961. Stress concentrations in filamentary structures, NASA TN D-882, NASA Langley Research Center.

Hedgepath, J.M., Van Dyke, P., 1967. Local stress concentrations in imperfect filamentary composite materials. J. Compos. Mater. 1, 294–305.

Hikami, F., Chou, T.-W., 1990. Explicit crack problem solutions of unidirectional composites: elastic stress concentrations. AIAA J. 28, 499–505.

Hulbert, L.E., Rybicki, E.F., 1971. Boundary point least squares analysis of the free edge effects in some unidirectional fiber composites. J. Compos. Mater. 5, 164–175.

Mindlin, R.D., Tiersten, H.F., 1962. Effects of couple-stresses in linear elasticity. Arch. Rat. Mech. Anal. 11, 415–448.

Mindlin, R.D., 1963. Influence of couple-stress on stress concentrations. Exp. Mech. 3, 1–7.

Muki, R., Sternberg, E., 1965. The influence of couple-stresses on singular stress concentration in elastic solids. Zeit. Angew. Math. Physik. 16, 611–648.

Nakamura, S., Benedict, R., Lakes, R.S., 1984. Finite element method for orthotropic micropolar elasticity. Int. J. Engng. Sci. 22, 319–330.

Pagano, N.J., 1974a. On the calculation of interlaminar normal stress in composite laminate. J. Compos. Mater. 8, 65–81.

Pagano, N.J., 1974b. The role of effective moduli in the elastic analysis of composite laminates. In: Sendeckyi, G.P. (Ed.), Mechanics of Composite Materials, vol. 2. Academic Press, New York, pp. 1–22.

Pagano, N.J., 1978. Free-edge stress fields in composite laminates. Int. J. Solids Struct. 14, 401–406.

Pagano, N.J., Rybicki, E.F., 1974. On the significance of effective modulus solutions for fibrous composites. J. Compos. Mater. 8, 214–228.

Pagano, N.J., Sih, G.C., 1968. Stress singularities around a crack in a cosserat plate. Int. J. Solids Struct. 4, 531–553.

Pagano, N.J., Yuan, F.G., 2000. Significance of effective modulus theory (homogenization) in composite laminate mechanics. Comp. Sci. Tech. 60, 2471–2488.

Pipes, R.B., Pagano, N.J., 1970. Interlaminar stresses in composite laminates under uniform axial extension. J. Compos. Mater. 4, 538–548.

Rybicki, E.F., Pagano, N.J., 1975. A study of the influence of microstructure on the modified effective modulus approach for composite laminates. Proceedings of the 1975 International Conference on Composite Materials (ICCM), vol. 2, pp. 149–159.

Savin, G.N., Nemish, Y.N., 1968. Investigations into stress concentration in the moment theory of elasticity (survey). Prikl. Mekh. 4, 1–17.

Schaefer, V.H., 1962. Versuch einer elastizitätstheorie des zweidimensionalen ebenen Cosserat-Kontinuums. In: Schäfer, M. (Ed.), Miszellanen der Angew. Mech. Akademie-Verlag, Berlin, pp. 277–292.

Sternberg, E., Muki, R., 1967. The effect of couple-Stresses on the stress concentration around a crack. Int. J. Solids Struct. 3, 69–95.

Sternberg, E., 1968. Couple-stresses and singular stress concentrations in elastic solids. In: Kröner, E. (Ed.), Mech. Generalized Continua. Springer-Verlag, New York, pp. 95–108.

Voigt, W., 1887. Theoretische studien uber die elasticitatsverhaltnisse der krystalle. Abhandlungen der Koniglichen Gesellschaft der Wissenschaften zu Gottingen, vol. 34.

Wang, S.S., Yuan, F.G., 1983. A hybrid finite element approach to composite laminate elasticity problems with singularities. J. Appl. Mech. 50, 835–844.

Wood, R.D., 1988. Finite element analysis of plane couple-stress problems using first order stress functions. Int. J. Numer. Meth. Engng. 26, 489–509.

Yuan, F.G., Pagano, N.J., Cai, X., 1997. Elastic moduli of brittle matrix composites with interfacial debonding. Int. J. Solids Struct. 34, 177–201.